

AD-A054 507

OCEANICS INC PLAINVIEW N Y

F/G 13/10

HYDRODYNAMIC ANALYSIS OF THE PERFORMANCE OF A MOORED HEMISPHERE--ETC(U)

MAY 76 P KAPLAN, J SCHNEIDER, H JASLOW

DOT-CG-53393-A

UNCLASSIFIED

76-125

USCG-D-99-76

NL

1 of 2
AD
A054507



AD A 054507

AD No. 1
DDC FILE COPY

18 19
Report No 4 SCG-D-99-76

FOR FURTHER TRAN *File*

12

6 HYDRODYNAMIC ANALYSIS OF THE PERFORMANCE
OF A MOORED HEMISpherical FAST WATER BUOY

10

Paul /Kaplan,
Jesse /Schneider,
Howard /Jaslow
Theodore R. /Goodman



11 May 1976

9 FINAL REPORT

12 106 P.

14 76-125

Document is available to the U. S. public through the
National Technical Information Service,
Springfield, Virginia 22161

15 DOT-CG-53393-A

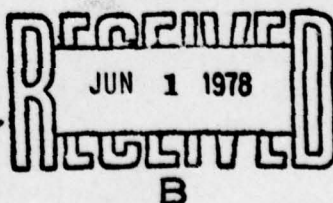
Prepared for

U. S. DEPARTMENT OF TRANSPORTATION

UNITED STATES COAST GUARD

Office of Research and Development
Washington, D.C. 20590

DDC

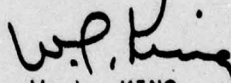


NOTICE

This document is disseminated under the sponsorship of the Department of Transportation in the interest of information exchange. The United States Government assumes no liability for its contents or use thereof.

The United States Government does not endorse products or manufacturers. Trade or manufacturers' names appear herein solely because they are considered essential to the object of this report.

The contents of this report do not necessarily reflect the official view or policy of the U. S. Coast Guard and do not constitute a standard, specification, or regulation.



W. L. KING
Captain, U. S. Coast Guard
Chief, Environmental and
Transportation Technology Division
Office of Research and Development
U. S. Coast Guard
Washington, D. C. 20590

DISCLAIMER NOTICE

**THIS DOCUMENT IS BEST QUALITY
PRACTICABLE. THE COPY FURNISHED
TO DDC CONTAINED A SIGNIFICANT
NUMBER OF PAGES WHICH DO NOT
REPRODUCE LEGIBLY.**

Technical Report Documentation Page

1. Report No. CG-D-99-76 ✓	2. Government Accession No.	3. Recipient's Catalog No.	
4. Title and Subtitle Hydrodynamic Analysis of the Performance of a Moored Hemispherical Fast Water Buoy		5. Report Date MAY 1976	
6. Author(s) Kaplan, Schneider, Jaslow, and Goodman		7. Performing Organization Code	
8. Performing Organization Name and Address Oceanics, Inc. Technical Industrial Park Plainview, New York 11803		9. Work Unit No. (TRAIL)	
10. Sponsoring Agency Name and Address Office of Research and Development US Coast Guard Washington, DC 20590		11. Contract or Grant No. DOT-CG-53393-A	
12. Sponsoring Agency Code G-DET-4		13. Type of Report and Period Covered Final Report	
14. Supplementary Notes			
15. Abstract This report describes in detail the development of a predictive technique for determining the optimum mooring attachment point for a hemispherical buoy in a swift-running river current. Representative analyses, which were performed to demonstrate the utility of the technique for observing trends and, in general, to give the user a feel for the impact of specific design parameters on the performance of such buoys, are included also. Finally, the authors offer conclusions and recommendations for follow-on work, particularly an expanded testing program which would yield more refined hydrodynamic data and, consequently, more accurate performance predictions.			
16. Key Words Buoys, Navigation Buoys, River Buoys, River Aids to Navigation, Fast Water Buoys		17. Distribution Statement Document is Available to the Public through the National Technical Information Service, Springfield, Virginia 22151	
18. Security Classif. (of this report) Unclassified	19. Security Classif. (of this page) Unclassified	20. No. of Pages 95	21. Price

263 650

PREFACE

This report is taken directly from Oceanics, Inc. report No. 76-125 entitled "Hydrodynamic Analysis of the Performance of a Moored Hemispherical Fast Water Buoy." It was prepared in partial fulfillment of Contract No. DOT-CG-53393-A for a study of the hydrostatic and hydrodynamic behavior of a hemispherical fast water buoy. It describes the effort in general, presents the results of the various analyses which were performed, and offers conclusions and recommendations for follow-on work.

ACCESSION for		
NTIS	White Section <input checked="" type="checkbox"/>	
DOC	Buff Section <input type="checkbox"/>	
UNARMED/ARMED <input type="checkbox"/>		
JUSTIFICATION		
BY		
DISTRIBUTION/AVAILABILITY CODES		
Dist. AVAIL. and/or SPECIAL		
A	23 88	

TABLE OF CONTENTS

	<u>Page</u>
NOMENCLATURE	iii
LIST OF TABLES	vi
LIST OF FIGURES.	vii
1.0 INTRODUCTION.	1
2.0 DESCRIPTION OF THE MATHEMATICAL MODEL	5
2.1 General Features.	5
2.2 The Cable System.	7
2.3 Determination of Buoy Equilibrium	14
2.3(a) Hydrodynamic Effects	14
2.4 Debris Attachment - The Effect of Concentrated Loads	19
2.4(a) The Broken Line Model.	19
2.4(b) The Clamped Mass Model	21
3.0 EVALUATION OF GEOMETRIC AND HYDROSTATIC PARAMETERS.	23
4.0 TEST PROGRAM AND RESULTS FOR HYDRODYNAMIC FORCE AND MOMENT MEASUREMENTS	28
4.1 Introduction.	28
4.2 Description of the Test Model	28
4.3 The Test Procedure - Test Conditions and Measurements.	29
4.4 Description of the Data Obtained and Its Reduction	32
5.0 VALIDATION OF THE MATHEMATICAL MODEL.	47
5.1 Introduction.	47

TABLE OF CONTENTS

	<u>Page</u>
5.2 The Characteristics of the Test Model	48
5.3 Test Set-Up and Procedure	50
5.4 The Range of Test Conditions and Measurements Taken	53
5.5 Results and Comparison with Numerical Predictions	54
6.0 PARAMETRIC STUDY RESULTS.	63
6.1 Introduction - Parameter Selection.	63
6.2 Discussion of the Results	67
6.3 Effect of Mooring Cable Scope	76
6.4 Effect of Variation of Cable Diameter	77
6.5 Effect of Variation of Cable Drag Coefficient	78
6.6 Effect of Cable Elasticity.	79
6.7 Effect of Debris Impingement on System Performance	81
7.0 ADDITIONAL EFFECTS.	86
7.1 Unsteady Effects.	86
7.2 Vortex Shedding	87
8.0 CONCLUSIONS AND RECOMMENDATIONS	90
8.1 Conclusions	90
8.2 Recommendations	92
9.0 REFERENCES.	93

NOMENCLATURE

A_c - cable cross-sectional area (i.e., load bearing area)

A_o - projected area of buoy at relative immersion $d/R = 1$,
i.e., semi-circular area.

A_p - submerged projected area of buoy

B - buoyant force acting on buoy

c - thickness of the cable cross-section in the plane
of the current

c_{Dc} - drag coefficient of the buoy

c_{Lc} - lift coefficient of the buoy

c_{Mc} - pitching moment coefficient of the buoy

c_R - drag coefficient of cable when cable is perpendicular
to flow

c_N - normal drag coefficient of cable

c_T - tangential drag coefficient of cable

d - buoy draft

d_B - buoy hull diameter

d_c - cable diameter

D_a - attachment drag

D_c - drag force acting on the buoy due to the current

D_{ca} - hydrodynamic drag on the cable

D_{CND} - cable drag without debris per section of cable length

e - constant used to evaluate the tangential drag
coefficient of the cable (depends upon cable
construction)

E_c	- effective static elastic modulus of cable material
f	- constant used to evaluate the tangential drag coefficient of the cable
F_N	- hydrodynamic force per unit length normal to the cable
F_r	- Froude number
F_T	- hydrodynamic force per unit length tangential to the cable
g	- acceleration due to gravity
GM	- buoy metacentric height
\overline{GZ}	- righting arm of buoy (see Equation (21))
h	- water depth
K_a	- drag constant for debris
K'	- percentage increase in cable drag due to debris
l_c	- cable length
L_c	- lift force acting on the buoy due to the current
M_c	- pitching moment acting on the buoy due to the current
r	- waterline radius of the buoy
R_a	- radial distance from buoy center to buoy-cable attachment point
R	- spherical radius of the buoy
s	- distance along the unstretched cable
t	- time
T	- cable tension
V_c	- current speed
V	- submerged volume of buoy
V_o	- submerged volume of buoy at a relative immersion $d/R = 1$, i.e., volume of the hemisphere

w_a - weight of the attachment in water

w_c - cable weight in water per unit length

w_b - total weight of the buoy

\bar{x} - see Equation (19)

x_c - horizontal coordinate of the cable attachment point at the buoy

y_o - constant in stress-strain relationship (see Equation (7))

\bar{z} - see Equation (20)

z_c - vertical coordinate of the cable attachment point at the buoy

$z_{c.g.}$ - vertical location of the buoy center of gravity measured positive upward from the bottom of the keel

α - cable attachment angle, measured at spherical center from buoy centerline positive upward from bottom center

β - inscribed angle of buoy geometry (see sketch page 21)

ϵ - cable strain

θ - pitch angle of buoy

π - physical constant

ρ - water density

τ - relaxation time constant in strain Equation (7)

ϕ - angle of cable with respect to the horizontal

LIST OF TABLES

<u>Table No.</u>		<u>Page</u>
1	Matrix of Test Conditions.	31
2	Matrix of Validation Test Runs	53
3	Test Results and Program Predictions . .	54
4	Revised Hemispherical Buoy - Cable System Parameters	63
5	Appropriate Parameter Combinations . . .	64
6	Current Speed - Depth - Cable Length . .	65
7	Relationship of Maximum Cable Tension To Buoy Draft.	70
8	Effect of Increased Buoy Weight on Equilibrium Draft at Fixed Current Speed	75
9	Mooring Cable Scopes	75
10	Effect of Mooring Cable Diameter	77
11	Effect of Cable Drag Coefficient	79
12	Effect of Cable Elasticity on System Performance.	80
13	Effect of Subsurface Debris Accumulation.	83
14	Effect of Debris at the Waterline. . . .	85

LIST OF FIGURES

<u>Figure No.</u>		<u>Page</u>
1	Buoy-Cable Coordinate Systems.	8
2	Cable Free-Body Diagram.	10
3	Nondimensional Properties of a Hemispherical Buoy	27
4	Sketch of the Test Model and Schematic of the Instrumentation	30
5(a)-5(f)	Photographs Taken at Various Test Conditions of Buoy Immersion and Simulated Current Speed.	33-38
6	Hydrodynamic Lift for a Hemispherical Buoy	39
7	Hydrodynamic Drag for a Hemispherical Buoy	40
8	Hydrodynamic Pitching Moment for a Hemispherical Buoy	41
9	Hydrodynamic Lift Coefficient for a Hemispherical Buoy	44
10	Hydrodynamic Drag Coefficient for a Hemispherical Buoy	45
11	Hydrodynamic Pitching Moment Coefficient For a Hemispherical Buoy	46
12	Model Outline.	49
13	Photo of Model in Workshop	49
14	Test Set-Up.	51
15	Photos Showing Details of Cable Attachment	52
16(a)-16(g)	Still-Photographs Taken to Determine Pitch Attitude of Buoy During Validation Tests.	55-61

LIST OF FIGURES
(Continued)

<u>Figure No.</u>		<u>Page</u>
17	Trim vs. Attachment Angle for Various Current Speeds	68
18	Trim vs. Metacentric Height for Various Buoy Diameters	69
19	Maximum Cable Tension vs. Attachment Angle	71
20	Maximum Cable Tension vs. Current Speed.	73
21	Maximum Cable Tension vs. Buoy Weight. .	74

1.0 INTRODUCTION

This report describes in detail the development of a predictive technique for determining the optimum mooring attachment point for a hemispherical buoy in a swift-running river current. The hemispherical hull form is the result of an extensive field testing program which was begun in the summer of 1972 by U. S. Coast Guard R & D personnel. Their objective was to find a hull shape which would survive the extremely adverse conditions which often exist on many of the navigable rivers in the Western River System of the United States. A complete description of the problem, the test program which was undertaken, and the results obtained from these field tests is presented in [1].

At times, river buoys are subjected to extremely high river currents which they may not survive. ("Survival" connotes remaining on station in good physical condition, i.e., continuing to provide the required navigational information.) Their survivability is challenged also by the accumulation of surface and sub-surface debris on the buoy and the mooring cable and by rapidly changing river levels. The hemispherical buoy was found to have satisfactory performance in all combinations of river current and debris accumulation encountered during the field tests. However, one problem which did arise during the tests of the buoys at the higher current speeds was their tendency to assume large running trim angles (equilibrium pitch angles), detracting from the effectiveness of their navigation signal.

The problem was associated with the fact that these original hemispherical designs used a point at the very bottom center of the keel for attachment of the mooring cable. A later generation of hemispherical buoys with side mooring attachment points were tested late in 1974. They demonstrated satisfactory performance in currents as high as 8 miles per hour [1].

Although it is possible to find an optimum mooring attachment point for any particular design and set of conditions empirically or by some cut-and-try approach, such a procedure has serious shortcomings when a variation of even a small number of physical characteristics of the buoy, cable, or river conditions are being considered. Hence, the overall objective of this study was to develop a design tool which, by some analytical means, would enable the user to predict the performance of a hemispherical buoy-cable system in a "fast water" environment for a wide variety of buoy characteristics and buoy/mooring configurations.

The specific objectives of the study were the following:

- 1) To develop a predictive design tool to determine the optimum mooring attachment point for a hemispherical buoy in high speed currents.
- 2) To provide some means of evaluating the sensitivity of the predicted optimum point to variations in drag due to debris accumulation.
- 3) To investigate possible buoy-cable system design constraints imposed by vibrations due to vortex shedding.

To accomplish these objectives a study program was undertaken which combined the elements of a mathematical analysis with a series of towing tank experiments and resulted in a predictive design tool in the form of a computer program.

Section 1.0 of this report describes the mathematical model developed to predict the performance of the hemispherical buoy-cable system in the river environment. The essential features of the model are discussed in detail. They include a discussion of the cable system, how buoy equilibrium is determined, and how hydrodynamic effects are incorporated into the model. Assumptions that have been made in the formulation of the model are clearly stated.

The report continues with a development of the geometric and hydrostatic parameters which are unique to a family of buoys which have a spherical-segment underwater hull form. The determination of the hydrodynamic parameters is made with the aide of a series of towing tank experiments on a hemispherical buoy model. These experiments are described in detail and the resulting data are presented.

Once the mathematical model was developed and a computer program was written to implement it, a series of towing tank tests were performed on the same hemispherical buoy model used for the towing tank experiments above for the purpose of validating the mathematical model. These tests are described in detail in Section 5.0 and comparisons with the computer-generated results for the same set of buoy, cable, and environmental conditions used during the tests are presented.

The next section of the report presents the results of an extensive parametric study made with the computer programs to determine the general performance of this type of buoy-cable system. The critical design parameters are indicated along with the effect of debris accumulation, cable elasticity, and cable drag variation.

The last technical section of the report contains a discussion of the influence of unsteady forces and vortex shedding on the performance of this type of buoy-cable system. The report concludes with a summary of the important findings of the study and some recommendations.

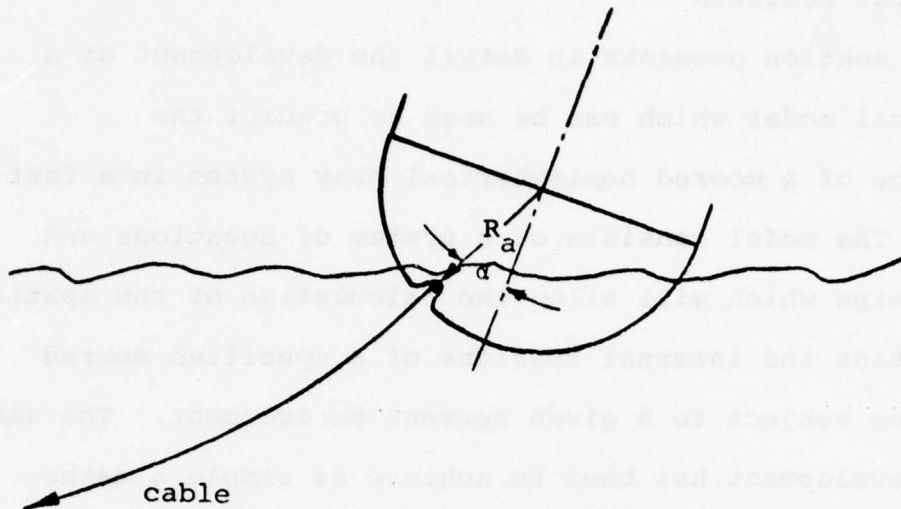
2.0 DESCRIPTION OF THE MATHEMATICAL MODEL

2.1 General Features

This section presents in detail the development of a mathematical model which can be used to predict the performance of a moored hemispherical buoy system in a fast current. The model consists of a system of equations and relationships which will allow the calculation of the spatial configuration and internal tensions of a specified moored buoy system subject to a given current environment. The aim in this development has been to achieve as simple a mathematical representation as possible, without omitting significant behavioral aspects. Another objective has been to keep computational problems to a minimum while revealing the significant moored buoy system characteristics and the critical parameters upon which they depend.

The mathematical model is based upon certain definite concepts of a moored buoy system. Only buoys whose underwater shape is hemispherical are considered in this model. The cable is attached to the buoy at a single point at a distance R_a from the spherical center. The attachment point can be inside the spherical section and, as such, the mathematical model can be used to treat the case of a buoy moored with a bridle, since a single attachment point lying inside the hemisphere can be placed, conceptually, midway between the bridle attachment points on the spherical surface to obtain the same dynamic effect. In addition, the attachment point can be offset from the buoy centerline by some

angular displacement α as illustrated in the sketch below.



The mooring cable is assumed to consist of a single material whose cross-sectional shape is circular and whose shape and diameter do not vary along its length. The entire cable is assumed to be immersed in the water and is considered to be elastic.*

The effects of the accumulation of weeds, grass, and other debris on the performance of the buoy-cable system are accounted for by considering the mooring cable to be a special type of compound mooring, i.e., a mooring where concentrated loads can be spaced at various locations along the cable.

The major environmental factor influencing the moored buoy system in its static equilibrium configuration is the current speed. The current is assumed to be unidirectional with the speed assumed to be invariant with depth. The

* For completeness, the effect of cable stretch is included in the above analysis. The computer program and program manual were originally written considering the cable to be inelastic but have been modified since then to include the effect of cable stretch.

assumption of unidirectionality implies that the static configuration of the cable system lies in one plane. Wind loads on the exposed hull and daymark are ignored in this model.

The static equilibrium analysis developed assumes that surface waves are absent (there is no time-varying excitation) and that the buoy and mooring cable are in static equilibrium. The static equations of the buoy-cable system constitute a two-point boundary value problem which is nonlinear and of second order. In addition, a weight or concentrated load along the cable will create discontinuities in both the cable tension and the cable orientation.

No limitations are placed upon the depth of water or upon the absolute size of the system components. The coordinate systems for the cable and the buoy are shown in Figure 1.

2.2 The Cable System

The basic analysis takes into account the steady hydrodynamic forces acting on the flexible elastic cable due to the current and includes the weight of the cable (in water) and the forces due to the buoy and another concentrated load on the cable. The current is assumed to be unidirectional, as mentioned in the preceding section. Since no other external forces are being considered, the mooring cable system lies in a plane parallel to the current direction.

The basic method of approach is to solve the differential equations of cable tension and angular displacement piecewise

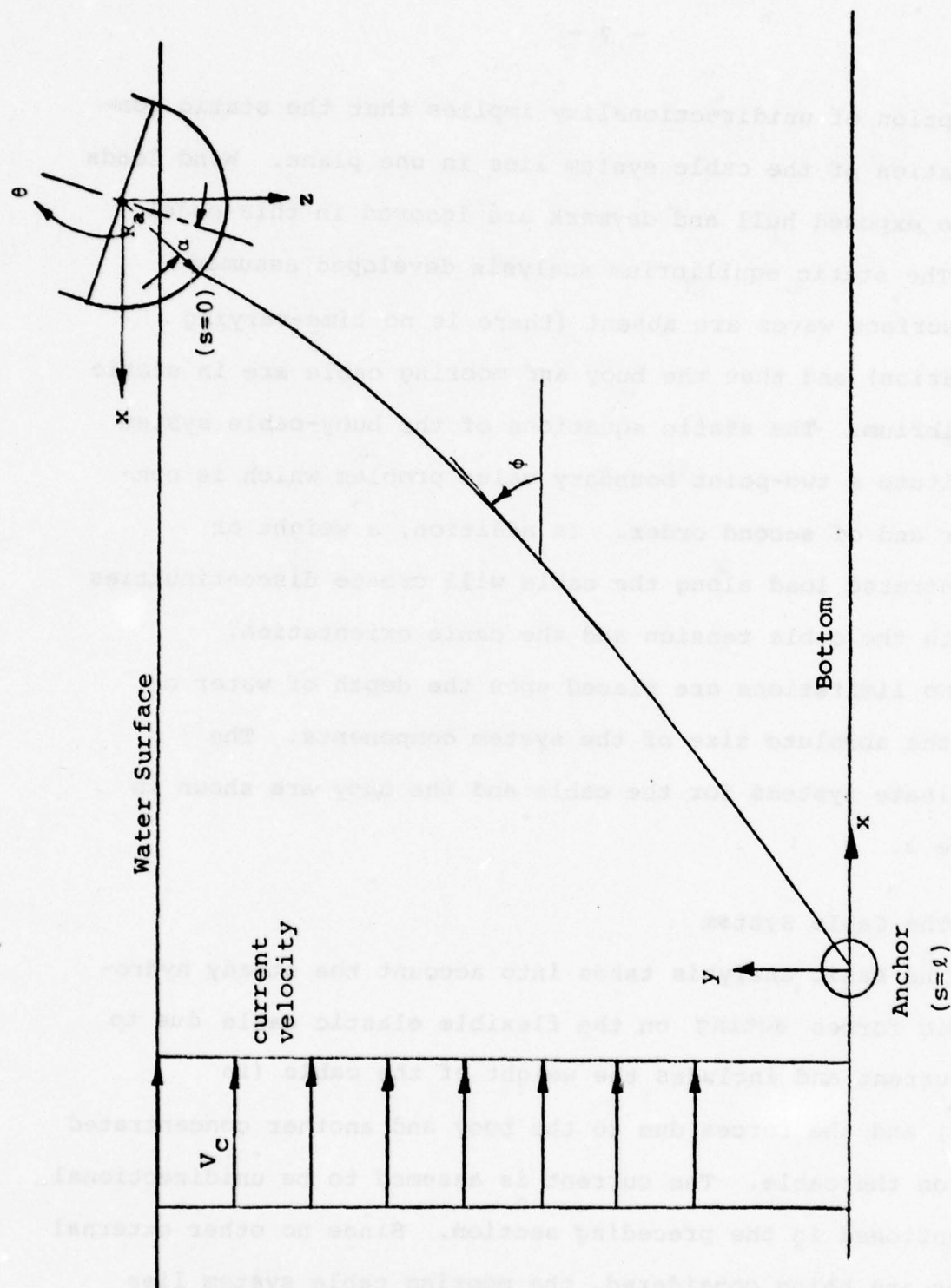


Figure 1. Buoy-Cable Coordinate Systems

for each section of the cable that is uniform between attachment points. The basic work in this area is by Pode [2] and Wilson [3] and has been applied and extended by Morrow and Chang [4] and by Schneider and Nickels [5].

The equations are developed with distance along the relaxed or unstretched cable, denoted by s , as the independent variable. Considering the static equilibrium problem, a free body diagram of a differential element of the cable in the plane of interest is shown in Figure 2. The cable bends and the tension varies along its length so as to keep all the forces in equilibrium. The cable weight acts vertically and the tension forces are directed along the cable axis.

The hydrodynamic forces due to the current are resolved into components normal and tangential to the cable direction. These unit forces are represented by

$$F_N = C_N \cdot \frac{1}{2} \rho c (V_c \sin \phi)^2 \quad (1)$$

and

$$F_T = C_T \cdot \frac{1}{2} \rho c (V_c \cos \phi)^2 \quad (2)$$

where ρ is the mass density of water

V_c is the current speed

c is the thickness of the cable cross section in the plane of the current and is the cable diameter for the case of a cable with a circular cross section.

ϕ is the angle of the cable with respect to the horizontal

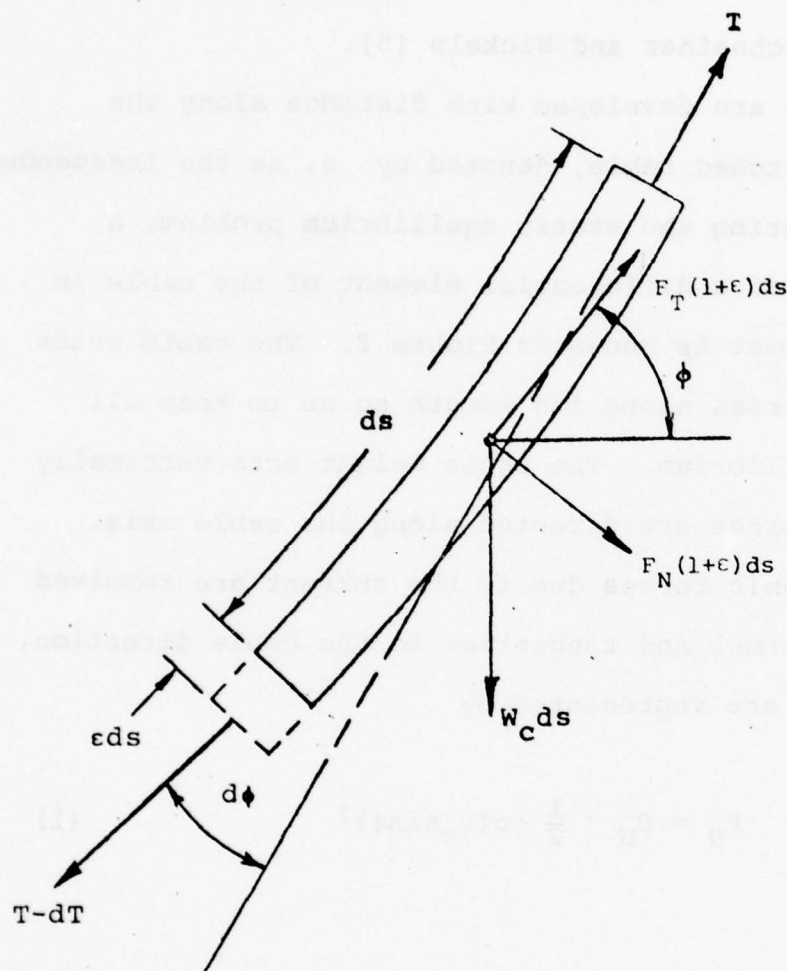


Figure 2. Cable Free-Body Diagram.

C_N and C_T are appropriate drag coefficients which depend upon the cross sectional shape of the cable, the material from which the cable is made, and the cable construction. Sufficient data exists in the literature to enable fairly reliable estimates of these coefficients to be made for a variety of cable types [6].

The summation of forces along the direction of the cable axis yields:

$$T + F_T(1+\epsilon)ds - w_c ds \sin\phi - (T-dT) \cos(d\phi) = 0 \quad (3)$$

where ϵ is the strain of the cable

w_c is the cable weight per unit length in water

ϕ is the angle of the cable with respect to the horizontal

and T is the tension in the cable

In the limit, the differential element $d\phi \rightarrow 0$ and, therefore, $\cos(d\phi) \rightarrow 1.0$. This results in the differential equation for the cable tension in terms of the distance along the relaxed cable, i.e., the independent variable s as follows:

$$\frac{dT}{ds} = [-F_T(1+\epsilon) + w_c \sin\phi] \quad (4)$$

The summation of forces normal to the cable axis results in

$$F_N(1+\epsilon)ds + W_C ds \cos\phi - (T-dT) \sin(d\phi) = 0 \quad (5)$$

Again, in the limit, as the differential element $d\phi \rightarrow 0$, the $\sin(d\phi)$ can be approximated by $d\phi$. Neglecting higher order terms, the above yields the equation for the differential angle $d\phi$ as follows.

$$\frac{d\phi}{ds} = \frac{1}{T} [F_N(1+\epsilon) + W_C \cos\phi] \quad (6)$$

The strain or cable elongation is obtained from the following relationship for an elastic cable material:

$$\tau Y_o \frac{\partial \epsilon}{\partial t} + A_C E_C \epsilon = T + \tau \frac{\partial T}{\partial t} \quad (7)$$

where A_C is the cable (load-bearing) cross sectional area
 E_C is the effective static elastic modulus of cable material

τ is a relaxation time constant

The above is based on a three-parameter Maxwell model and was originally derived by Reid in [7]. For the static (i.e., steady state) case, Equation (7) reduces simply to

$$\epsilon = \frac{T}{A_C E_C} \quad (8)$$

The horizontal displacement and depth of the cable are found from

$$\frac{\partial x}{\partial s} = (1+\epsilon) \cos\phi \quad (9)$$

$$\frac{\partial y}{\partial s} = (1+\epsilon) \sin\phi \quad (10)$$

The steady current flow considered in the static equilibrium condition exerts drag forces upon the cable elements as well as on the buoy and other mooring attachments.

The drag forces on the cable elements are given in Equations (1) and (2) in terms of drag coefficients. Only the circular cable is considered in this analysis, and for this case c =cable diameter and it is shown by Whicker [8] that C_N and C_T are given by

$$C_N = C_R \quad (11)$$

where C_R = drag coefficient when cable is perpendicular to the flow (≈ 1.2 for a circular cable) and

$$C_T = C_R (f + e/\cos\phi) \quad (12)$$

where f and e are coefficients which depend upon cable shape and surface construction. Based on two experimental results, it was found for circular cable that $f=-.035$ and $e=.083$. For cables

having other cross-sections C_N is dependent on ϕ .

In general, for the static case with an arbitrary current, it is necessary to solve Equations (1), (2), (4), (6), (8), and (10) simultaneously subject to certain boundary conditions at the buoy which arise from considering buoy-cable equilibrium and certain other boundary conditions at the anchor. These boundary conditions are presented in the following section and the means of integrating the equilibrium equations of the cable subject to these conditions is also described.

2.3 Determination of Buoy Equilibrium

In order to determine the cable boundary conditions at the buoy, the equilibrium configuration of the buoy must be determined first. The forces acting on the buoy include the buoy weight, the buoyant force, the cable tension at the cable attachment point and the hydrodynamic forces, i.e., the current-induced lift and drag. The moment acting on the buoy is composed of a hydrostatic contribution, a current-induced pitching moment, and a moment due to the tension in the cable at the buoy-cable attachment point. Each of these contributions is discussed below.

2.3(a) Hydrodynamic Effects

The steady current-induced forces and moments on a buoy or on any cable attachments such as debris are best determined through the use of experimental data. In addition, it is important that such data be properly scaled

to account for Reynolds number or Froude number effects. For the case of debris, Hoerner [9] presents compilations of such data for a wide variety of shapes. For the hemispherical buoy itself, an experimental program was conducted; measurements were made of the appropriate hydrodynamic quantities for a wide range of buoy drafts and towing (current) speeds. These data were normalized with respect to the test model geometry and current speed so as to properly account for Froude number effects. The test data and the methods used to scale them are described in detail in Section 4.0 of this report.

The buoy hydrodynamic forces and moments in the plane of interest are represented as:

$$D_c \equiv \text{Drag force induced by the current} = C_{D_c} \cdot \frac{1}{2} \rho V_c^2 A_p \quad (13)$$

(positive in direction of current)

$$L_c \equiv \text{Vertical force induced by the current} = C_{L_c} \cdot \frac{1}{2} \rho V_c^2 A_p \quad (14)$$

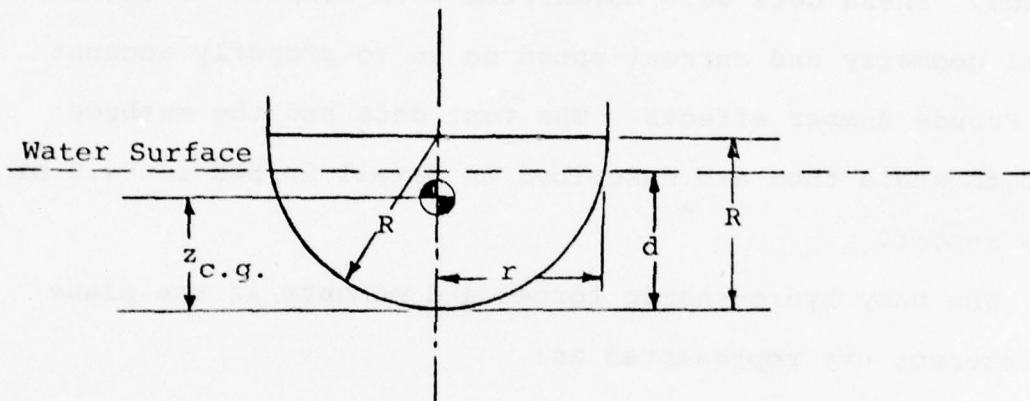
(positive downward)

$$M_c \equiv \text{Pitching moment induced by the current} = C_{M_c} \cdot \frac{1}{2} \rho V_c^2 A_p \cdot 2r \quad (15)$$

(positive from the upward-directed vertical towards the direction to which the current is flowing)

where A_p is the underwater projected area of the buoy and r is the waterline radius (see sketch below) C_D , C_L , and C_M are the hydrodynamic drag, lift, and pitching moment

coefficients, respectively; and they are all functions of the relative immersion d/R of the buoy and the Froude number $V_c/\sqrt{2gr}$, where R is the buoy radius (radius of the effective sphere) and d is the buoy draft (see sketch below).



These data are presented in Section 4.0.

Now, for static equilibrium of the buoy, all of the current-induced forces acting on the buoy must be in equilibrium with the buoy weight, buoyancy, and cable forces. These lead to the following force relationships:

$$D_C = T \cdot \cos\phi \quad (16)$$

and

$$L_C = B - W_B - T \cdot \sin\phi \quad (17)$$

where W_B is the total weight of the buoy and B is the buoyant force on the buoy which depends upon the buoy draft d . The evaluation of the geometric and

hydrostatic parameters for a buoy with a specific hemispherical underwater shape is described in Section 3.0.

The remaining consideration for static equilibrium of the buoy concerns moment equilibrium. For the case of a spherical buoy, any diameter is an axis of rotational (geometric) symmetry. Further, the metacenter lies at the intersection of these axes of rotational symmetry. Consequently, it is convenient to write the moment equilibrium equation about the metacenter since all pressure forces pass through it and are, thus, eliminated from the equation. The summation of moments about the buoy metacenter in the plane of interest results in the following relationship:

$$M_C = T \sin \phi \bar{X} - T \cos \phi \bar{Z} + w_B \bar{GZ} \quad (18)$$

with

$$\bar{X} = x_C \cos \theta + z_C \sin \theta \quad (19)$$

$$\bar{Z} = z_C \cos \theta - x_C \sin \theta \quad (20)$$

$$\bar{GZ} = (R - z_{c.g.}) \sin \theta \quad (21)$$

where θ is the running trim angle of the buoy

R is the buoy radius, i.e., the radius of the effective sphere

$z_{c.g.}$ is the vertical location of the buoy center of gravity measured positive upward from the buoy bottom.

The coordinates of the cable attachment point, x_c and z_c are given by:

$$x_c = R_a \cdot \sin\alpha \quad (22)$$

and

$$z_c = R_a \cdot \cos\alpha \quad (23)$$

where R_a is the radial distance from the sphere center to the attachment point and α is the angle of the cable attachment to the buoy measured positive upward from the bottom center of the buoy as shown in Figure 1.

The manner in which the static cable Equations (1), (2), (4), (6), and (10) are solved subject to the conditions represented by Equations (16), (17), and (18) is as follows: Equations (16) - (18) constitute three equations for the four unknowns T , ϕ , θ , d . A buoy draft is assumed and the three equations are solved for the three other quantities. The calculated values of T and ϕ then serve as initial conditions and are used to solve the cable equations. The integration proceeds down along the cable until one of three things happens:

- 1) the end of the cable is reached before the bottom

- 2) the bottom is reached before the end of the cable
- 3) zero slope is achieved before the bottom is reached

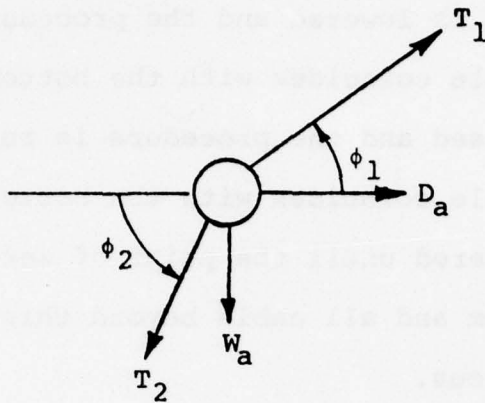
In case (1) the buoy is lowered and the procedure is repeated until the end of the cable coincides with the bottom. In case (2) the buoy is raised and the procedure is repeated until the end of the cable coincides with the bottom. In case (3) the buoy is lowered until the point of zero slope coincides with the bottom and all cable beyond this point is then essentially superfluous.

2.4 Debris Attachment - The Effect of Concentrated Loads

When a concentrated mass is attached to the cable its effect will be to add a point weight and point drag, and this will cause a discontinuity in the cable angle ϕ and in the tension T . The problem is to determine the amount by which these quantities jump at the point of such concentrated loads. For this purpose two models of the concentrated mass on the cable are postulated. In the first model the cable is considered to be broken and the point mass constitutes the connecting link between the two parts of the cable. In the second model the cable is considered to be continuous and the point mass is clamped to the cable. Both models will be presented and it will be shown that, although the equilibrium equations from each model are different, to second order in the concentrated loads, both models yield the same result.

2.4(a) The Broken Line Model

Consider the concentrated mass shown in the sketch below.



Sketch of Broken Line Model

Here D_a is the hydrodynamic drag and W_a is the weight of the concentrated mass. Upon considering the balance of forces in the horizontal and vertical directions, the following is obtained:

$$\begin{aligned} D_a + T_1 \cos\phi_1 - T_2 \cos\phi_2 &= 0 \\ W_a + T_2 \sin\phi_2 - T_1 \sin\phi_1 &= 0 \end{aligned} \tag{A.1}$$

Solving for ϕ_2 and T_2 results in

$$\tan\phi_2 = \frac{T_1 \sin\phi_1 - W_a}{T_1 \cos\phi_1 + D_a} \tag{A.2}$$

$$T_2^2 = W_a^2 + D_a^2 + T_1^2 + 2T_1 (D_a \cos\phi_1 - W_a \sin\phi_1) \tag{A.3}$$

For small concentrated loads let $\phi_2 = \phi_1 + \Delta\phi$, $T_2 = T_1 + \Delta T$ and expand. Then to second order it is found that

$$\Delta\phi = \frac{-(W_a \cos\phi_1 + D_a \sin\phi_1)}{T_1} \left[1 \pm \frac{D_a \cos\phi_1 - W_a \sin\phi_1}{T_1} \right] \quad (A.4)$$

$$\Delta T = (D_a \cos\phi_1 - W_a \sin\phi_1) \pm \frac{1}{2T_1} (D_a \sin\phi_1 + W_a \cos\phi_1)^2 \quad (A.5)$$

where the upper signs are to be used with subscript 1 and the lower signs with subscript 2. The choice of subscripts is dictated by the direction in which the cable equation is being integrated.

2.4(b) The Clamped Mass Model

For this model the differential equations for the cable are considered to be valid throughout, and the concentrated mass is represented by a Dirac delta function. The differential equations are then integrated across the point load to obtain the jump conditions.

From Equations (4) and (6) the differential equations are

$$\begin{aligned} \frac{dT}{ds} &= -D_{ca} \cos\phi + W_c \sin\phi \\ T \frac{d\phi}{ds} &= D_{ca} \sin\phi + W_c \cos\phi \end{aligned} \quad (B.1)$$

where the components of the hydrodynamic drag on the cable replace the normal and tangential hydrodynamic force components and where the strain has been set equal to zero in the immediate vicinity of a concentrated load. Upon letting $D_{ca} = D_a \delta(s-s_1)$, $W_c = W_a \delta(s-s_1)$ and postulating that T and ϕ undergo a step

from conditions 1 to conditions 2 there is obtained

$$\Delta T = D_a \left(\frac{\cos\phi_1 + \cos\phi_2}{2} \right) + w_a \left(\frac{\sin\phi_1 + \sin\phi_2}{2} \right) \quad (B.2)$$

and

$$- \left(\frac{T_1 + T_2}{2} \right) \Delta\phi = D_a \left(\frac{\sin\phi_1 + \sin\phi_2}{2} \right) + w_a \left(\frac{\cos\phi_1 + \cos\phi_2}{2} \right)$$

It can be seen immediately that these equations are not the same as Equations (A.1) since in Equations (A.1) the angles ϕ_1 and ϕ_2 appear only inside trigonometric functions, which is not the case here. On the other hand, if Equations (B.2) are expanded to the second order in the loads the results can be shown to be identical to Equations (A.4) and (A.5). It follows that the mathematical model chosen to represent the concentrated loads is not critical, and in practice Equations (A.3) and (A.4) have been incorporated into the computer program. The hydrodynamic drag is specified in each case by giving the value of K_a and defining the drag to be $D = K_a V_c^2$.

3.0 EVALUATION OF GEOMETRIC AND HYDROSTATIC PARAMETERS

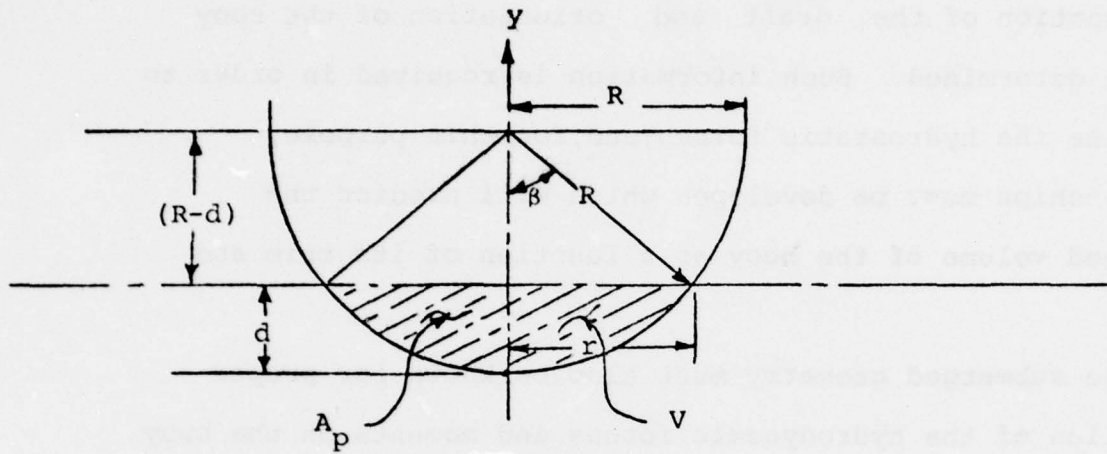
For a buoy of arbitrary shape, the submerged geometry as a function of the draft and orientation of the buoy must be determined. Such information is required in order to determine the hydrostatic forces; and, for this purpose, relationships must be developed which will predict the submerged volume of the buoy as a function of its trim and draft.

The submerged geometry must also be known for proper evaluation of the hydrodynamic forces and moments on the buoy since these depend upon the submerged projected area and the length at the waterline. The section which follows develops the necessary relationships for the specific buoy configuration under investigation in this study.

As mentioned before, for a spherical buoy, the metacenter is a point about which rotational symmetry exists and this fact is used to advantage in the analysis which follows. The single most important assumption upon which this analysis is based is that the submerged portion of the hemispherical buoy always remains a segment of a sphere regardless of the relative immersion of the buoy or its trim orientation. Clearly, for certain large values of trim, this assumption will be violated. However, these large values of trim are not of interest as acceptable equilibrium conditions in this study.

With this assumption in mind, using the sketch below, the radial distance from the vertical to the outside surface of the buoy at the waterline (referred to as the waterline

radius r) may be found from the geometry, i.e.,



$$(R-d)^2 + r^2 = R^2 \quad (24)$$

so that

$$r = \sqrt{d(2R-d)} \quad (25)$$

The volume of the submerged spherical segment then becomes the result of the single integral given by:

$$V = \int_0^d \pi r^2 dy = \int_0^d \pi y(2R-y) dy = \pi \left[Ry^2 - \frac{1}{3}y^3 \right]_0^d \quad (26)$$

$$V = \pi d^2 \left(R - \frac{d}{3} \right) \quad (27)$$

Nondimensionalizing the submerged volume with respect to the volume of the hemispherical section, $V_o = \frac{2}{3}\pi R^3$, (where V_o is obtained by merely changing the upper limit of integration in Equation (26) to R) results in:

$$\frac{V}{V_o} = \frac{3}{2} \left(\frac{d}{R} \right)^2 \left(1 - \frac{1}{3} \frac{d}{R} \right) \quad (28)$$

The waterline radius will also be more useful in non-dimensional form. Normalizing Equation (25) with respect to the buoy radius, R , results in

$$\frac{r}{R} = \sqrt{\frac{d}{R} (2 - \frac{d}{R})} \quad (29)$$

The remaining geometric information required is the value of the submerged projected area, A_p . Again, referring to the sketch on the previous page, the submerged projected area is simply the difference between the area of the circular sector prescribed by the angle (2β) and the radial distance R and the area of the isosceles triangular section of base $2r$, i.e.,

$$A_p = \beta R^2 - (R-d) r \quad (30)$$

Nondimensionalizing this with respect to the semicircular area, $A_o = \frac{\pi}{2} R^2$ gives

$$\frac{A_p}{A_o} = \frac{2}{\pi} \left[\beta - \left(1 - \frac{d}{R}\right) \frac{r}{R} \right] \quad (31)$$

The angle, β , can be rewritten in terms of inverse trigonometric functions such that

$$\beta = \sin^{-1} \left(\frac{r}{R} \right) \quad (32)$$

using this in Equation (31) results in the final expression for the normalized submerged projected area i.e.,

$$\frac{A_p}{A_o} = \frac{2}{\pi} \left[\sin^{-1} \left(\frac{r}{R} \right) - \left(1 - \frac{d}{R}\right) \frac{r}{R} \right] \quad (33)$$

The nondimensional submerged volume, submerged projected area and waterline radius are calculated for different levels of the relative immersion, d/R , and are plotted against that parameter in Figure 3.

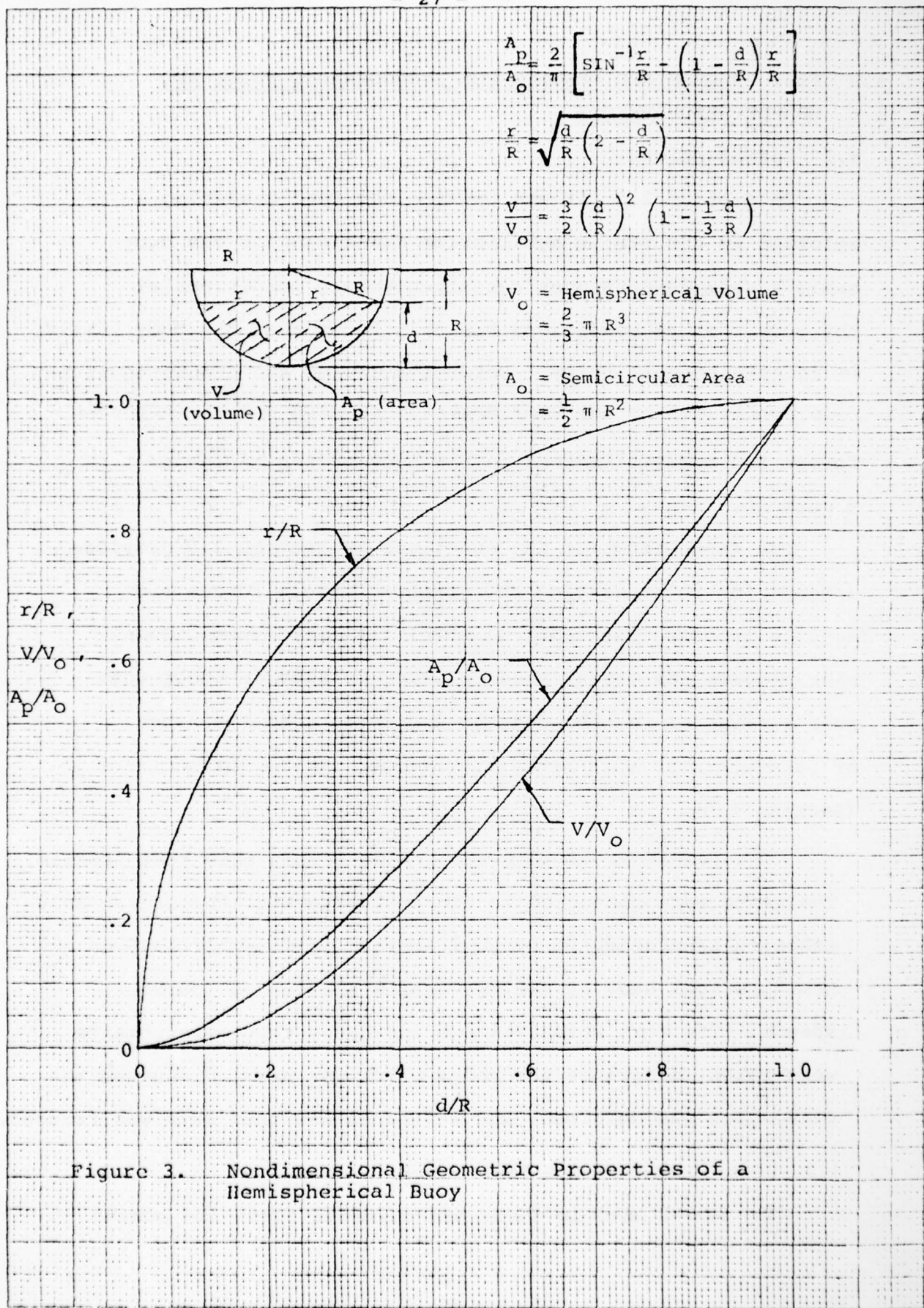


Figure 3. Nondimensional Geometric Properties of a Hemispherical Buoy

4.0 TEST PROGRAM AND RESULTS FOR HYDRODYNAMIC FORCE AND MOMENT MEASUREMENTS

4.1 Introduction

In Section 2.0 it was pointed out that obtaining a solution to the static equilibrium equations for the buoyable system depends upon certain boundary conditions at the buoy. These conditions are only known when the buoy itself is in static equilibrium. Determination of the static equilibrium conditions on the buoy requires knowing the hydrodynamic forces and moments induced on the buoy by the action of a current.

The formulation of the equations in Section 2.0 provides a means for incorporating the effect of these forces and moments into the mathematical model. A hydrodynamic model test program was established in order to provide these data over a range of test conditions appropriate to the range of parameters in this study, as outlined in the Introduction (Section 1.0).

The remainder of this section describes this test program. The tests were conducted in the towing tank at the Danish Ship Research Laboratory in Lyngby, Denmark in November 1975 on a hemispherical buoy at various drafts and towing (current) speeds. The text which follows indicates what measurements were taken, describes the model which was used, discusses the data which was obtained, and indicates how that data was reduced.

4.2 Description of the Test Model

The model used in these hydrodynamic force and moment

tests is illustrated in Figure 4 along with a schematic of the instrumentation set up to record the desired data. The model was a 3 foot diameter hemispherical buoy constructed from wood. A deck was set on top of the hemispherical section and extended a dimension of $R/4$ or $4 \frac{1}{2}$ " above the top of the hemisphere. This section of the model housed various instrumentation components and the major hardware by which the model was connected to the towing tank carriage. The deck area and the instrumentation and connecting hardware it contained was protected from water spray during the testing by a spray guard which extended above the deck approximately 10 inches.

4.3 The Test Procedure - Test Conditions and Measurements

By taking advantage of the rotational symmetry associated with a spherically shaped buoy, as discussed in Section 2.0, the test program required to obtain the necessary hydrodynamic force and moment data was considerably simplified. By referring the data obtained from the towing tank measurements to the metacenter, these data became independent of the trim angle and, as a consequence, trim angle did not have to be considered in the general matrix of test variables.

The test matrix was composed of only two parameters, the buoy draft nondimensionalized with respect to the buoy radius, and the towing (current) speed. Table 1 below presents the matrix of these test conditions.

Three sets of measurements were taken during each test

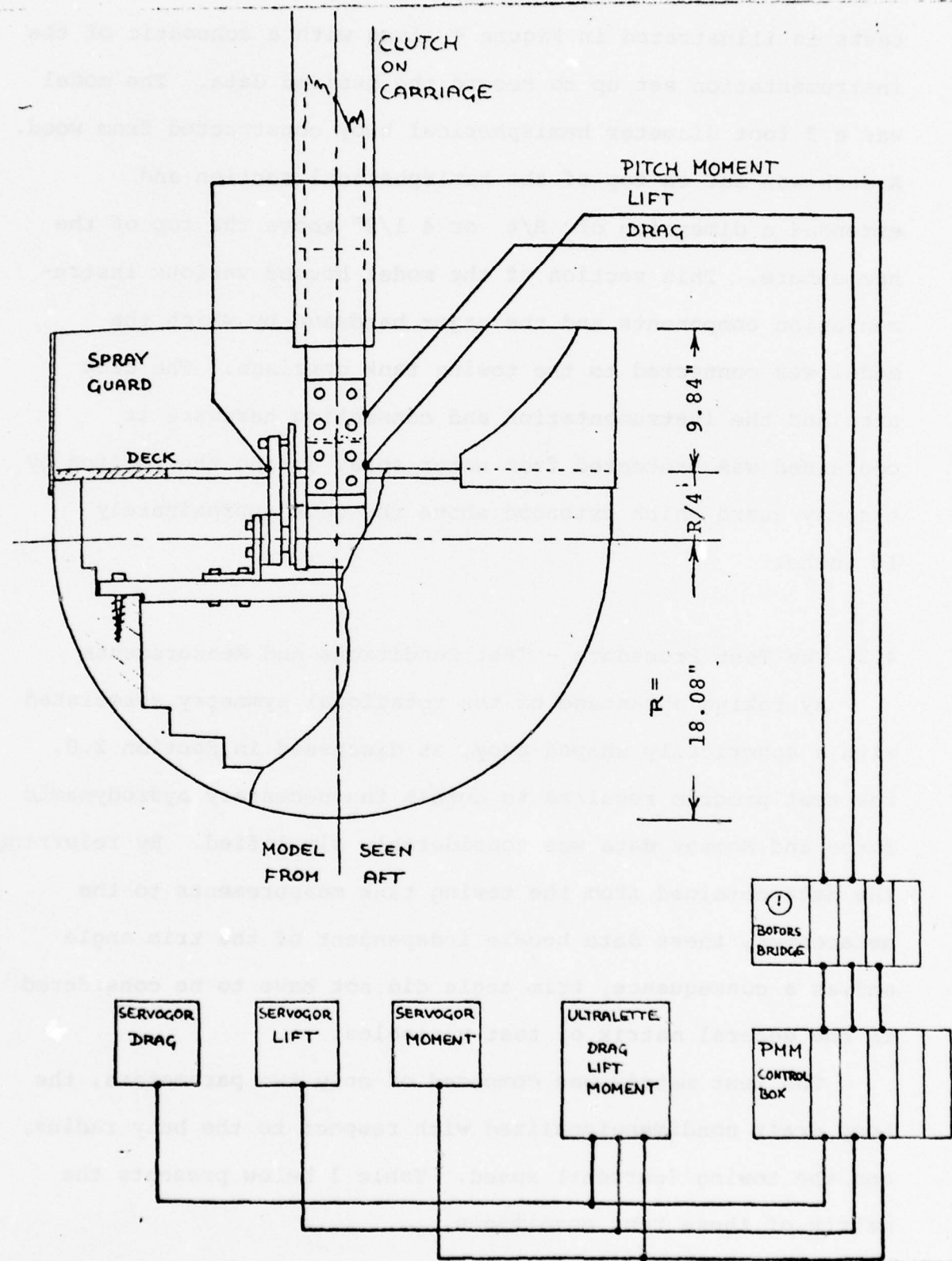


Figure 4. Sketch of the Test Model and Schematic of the Instrumentation.

TABLE 1
MATRIX OF TEST CONDITIONS

Towing (Current) Speed, V_c		Relative Immersion, d/R
fps	mph	
14.0	9.545	1/4
12.0	8.182	1/2, 1/4
10.0	6.818	3/4, 1/2, 1/4
8.0	5.454	1, 3/4, 1/2, 1/4
6.0	4.091	1, 3/4, 1/2
4.0	2.727	1, 3/4
1.0	0.682	1

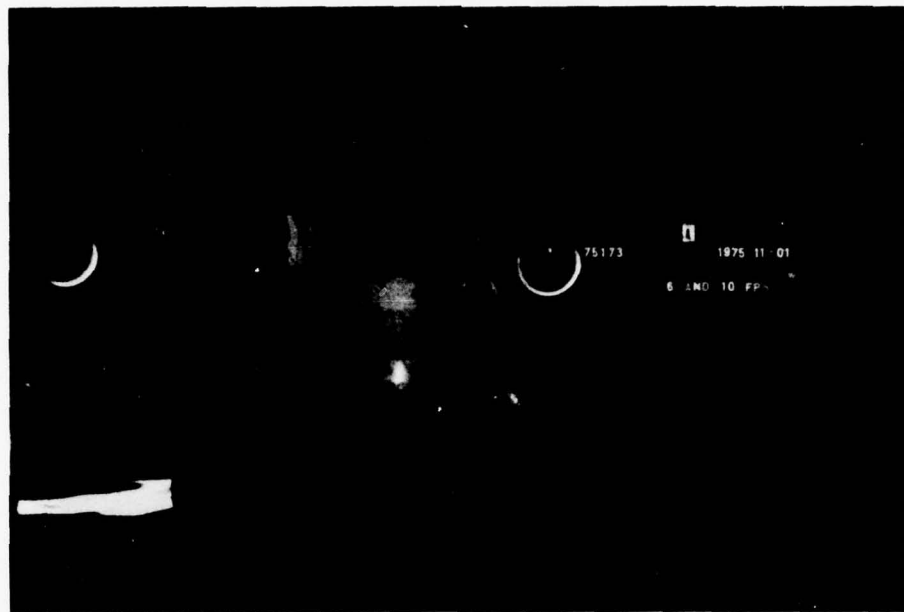
run. The total drag force on the buoy was recorded by a sensor located above the model center, as shown in Figure 4. The lift on the buoy was also obtained from a sensor located above the model center and was measured positive in the downward direction. The pitch moment was measured about the horizontal athwartship axis through the buoy center and was considered positive when it tended to lift the "bow" of the buoy model. The location of the moment sensor is also shown in Figure 4. The signals (Ultralette optical galvanometer recorder) shown in Figure 4 were recorded for all force and moment measurements and served only as a means to check the high-frequency periodic forces which act on the model during any portion of the testing sequence.

For each draft considered in the test matrix the model was ballasted so that the lift force would not exceed the maximum gauge load. However, during all runs, the buoy was completely restrained in relation to the test carriage.

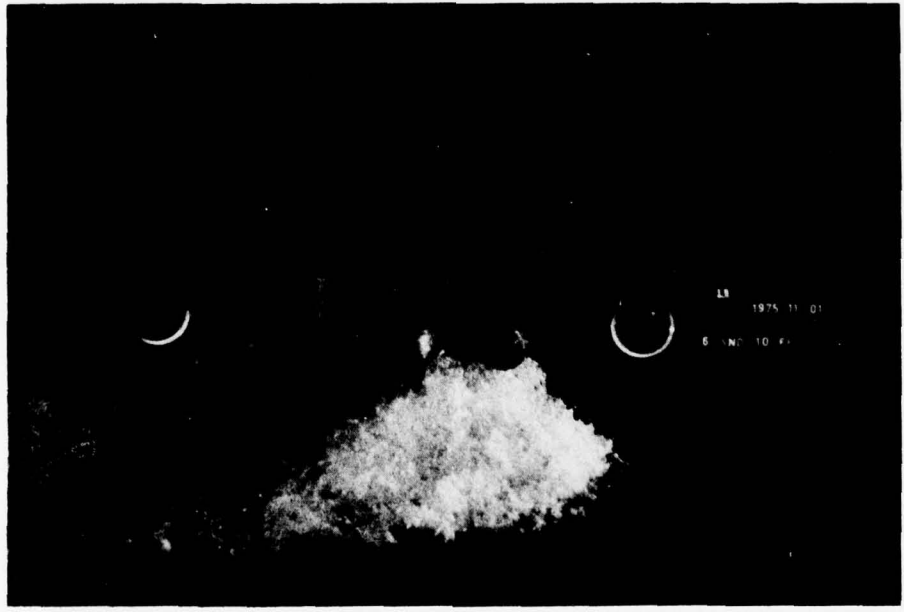
Figure 5(a) - 5(f) are photographs of the model taken during a number of test runs at various levels of buoy immersion and simulated current speed.

4.4 Description of the Data Obtained and Its Reduction

The current-induced lift, drag, and pitch moment on the hemispherical buoy model shown in Figure 4 are plotted against simulated current speed in Figure 6, 7, and 8, respectively. The varying parameter in each figure is the relative immersion of the buoy d/R , i.e., the draft of the buoy non-dimensionalized with respect to the buoy radius.

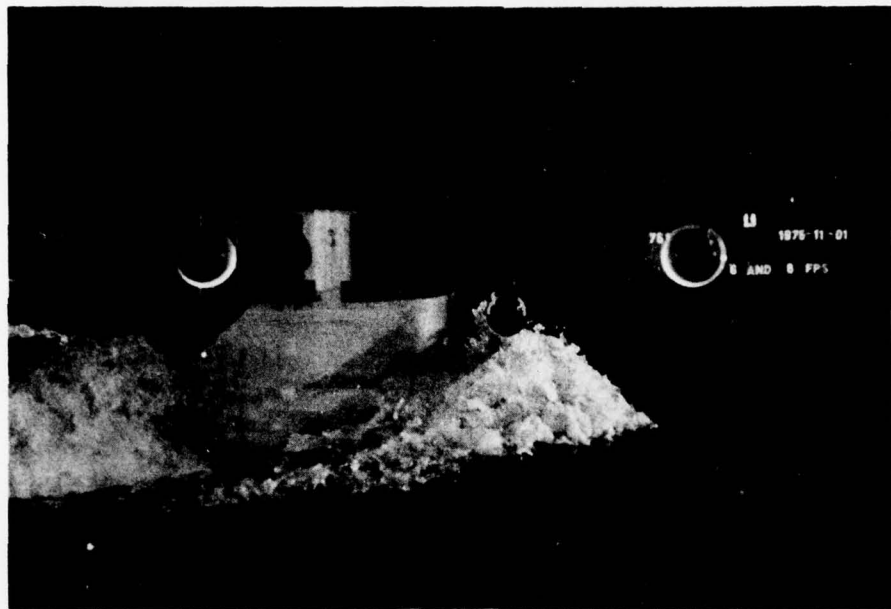


Run 6a, Draft = 3R/4 Speed 6 Feet Per Second



Run 6b, Draft = 3R/4 Speed 10 Feet Per Second

Figures 5(a)-5(f). Photographs Taken at Various Test Conditions
of Buoy Immersion and Simulated Current Speed



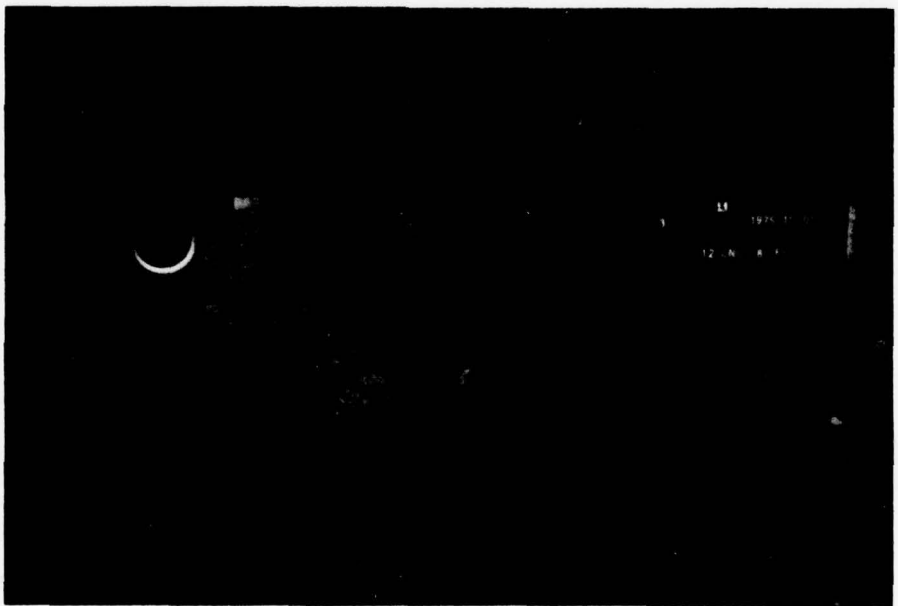
Run 7a, Draft = R Speed 8 Feet Per Second



Run 7b, Draft = R Speed 6 Feet Per Second

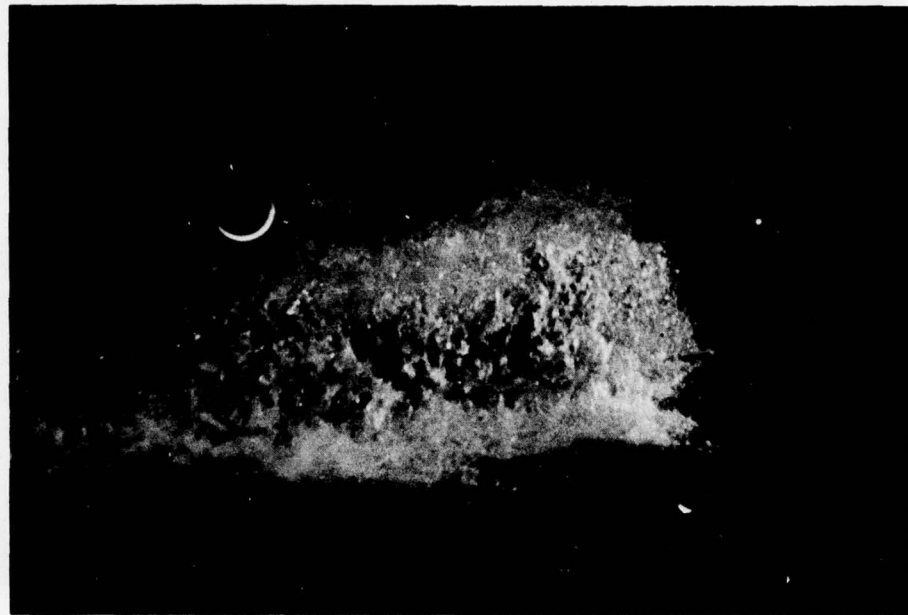


Run 9a, Draft = R/2 Speed 12 Feet Per Second

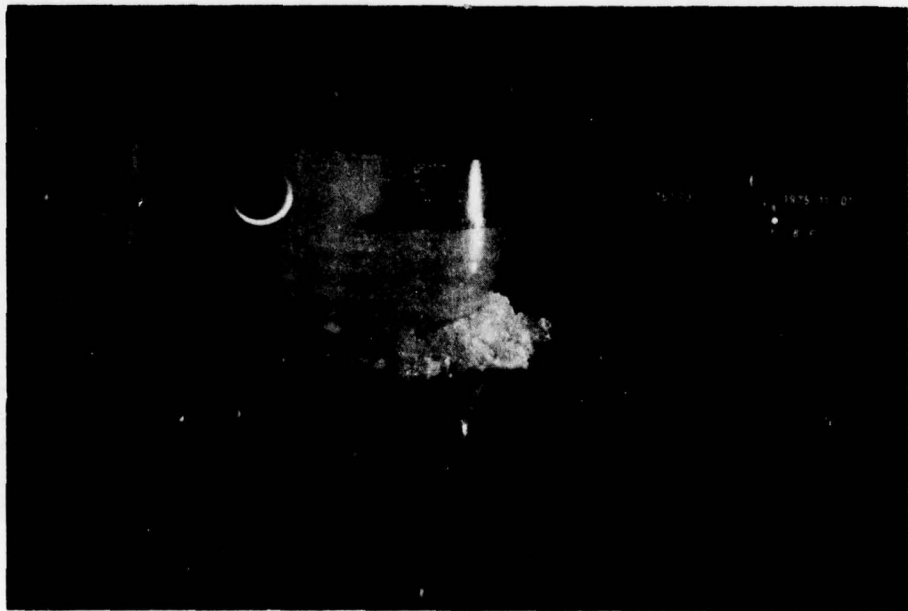


Run 9b, Draft = R/2 Speed 8 Feet Per Second

Figure 5(c)



Run 10a, Draft = $R/4$ Speed 14 Feet Per Second

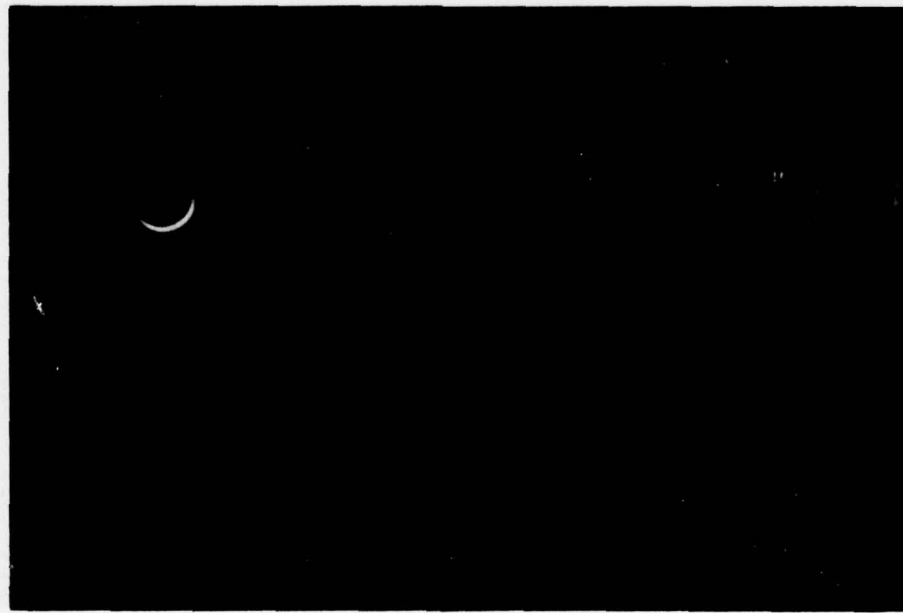


Run 10b, Draft = $R/4$ Speed 8 Feet Per Second

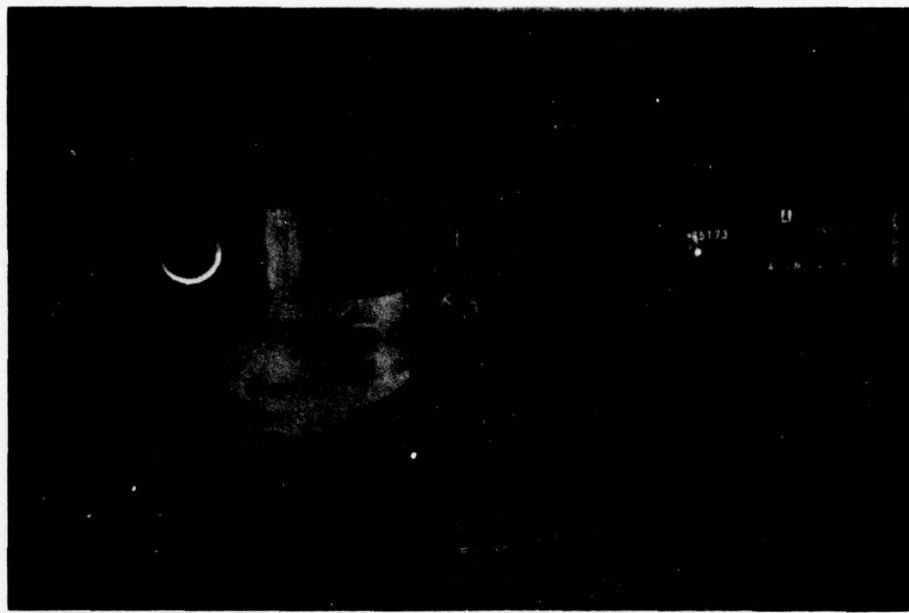
Figure 5(d)



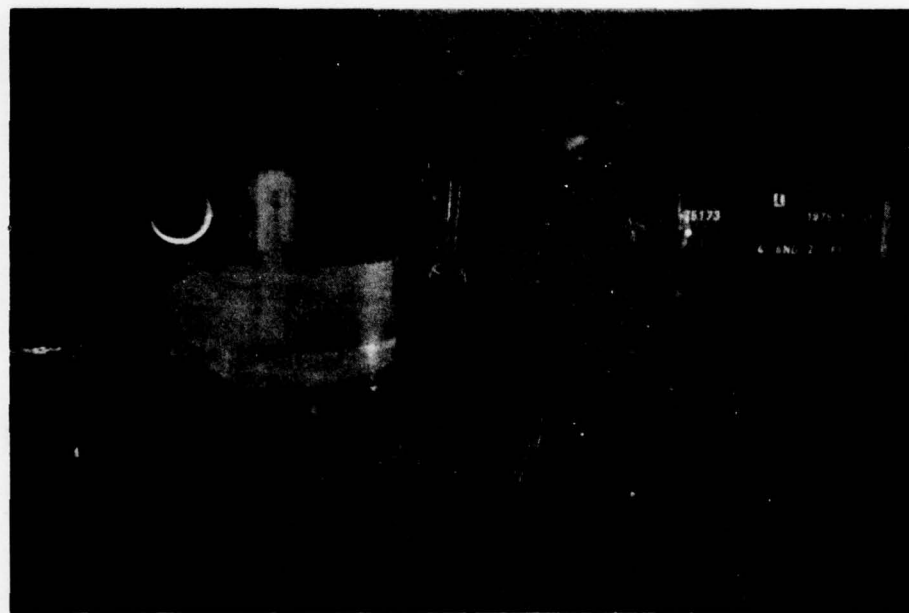
Run 11a, Draft = $R/4$ Speed 12 Feet Per Second



Run 11b, Draft = $R/4$ Speed 10 Feet Per Second



Run 12a, Draft = R Speed 4 Feet Per Second



Run 12b, Draft = R Speed 2 Feet Per Second

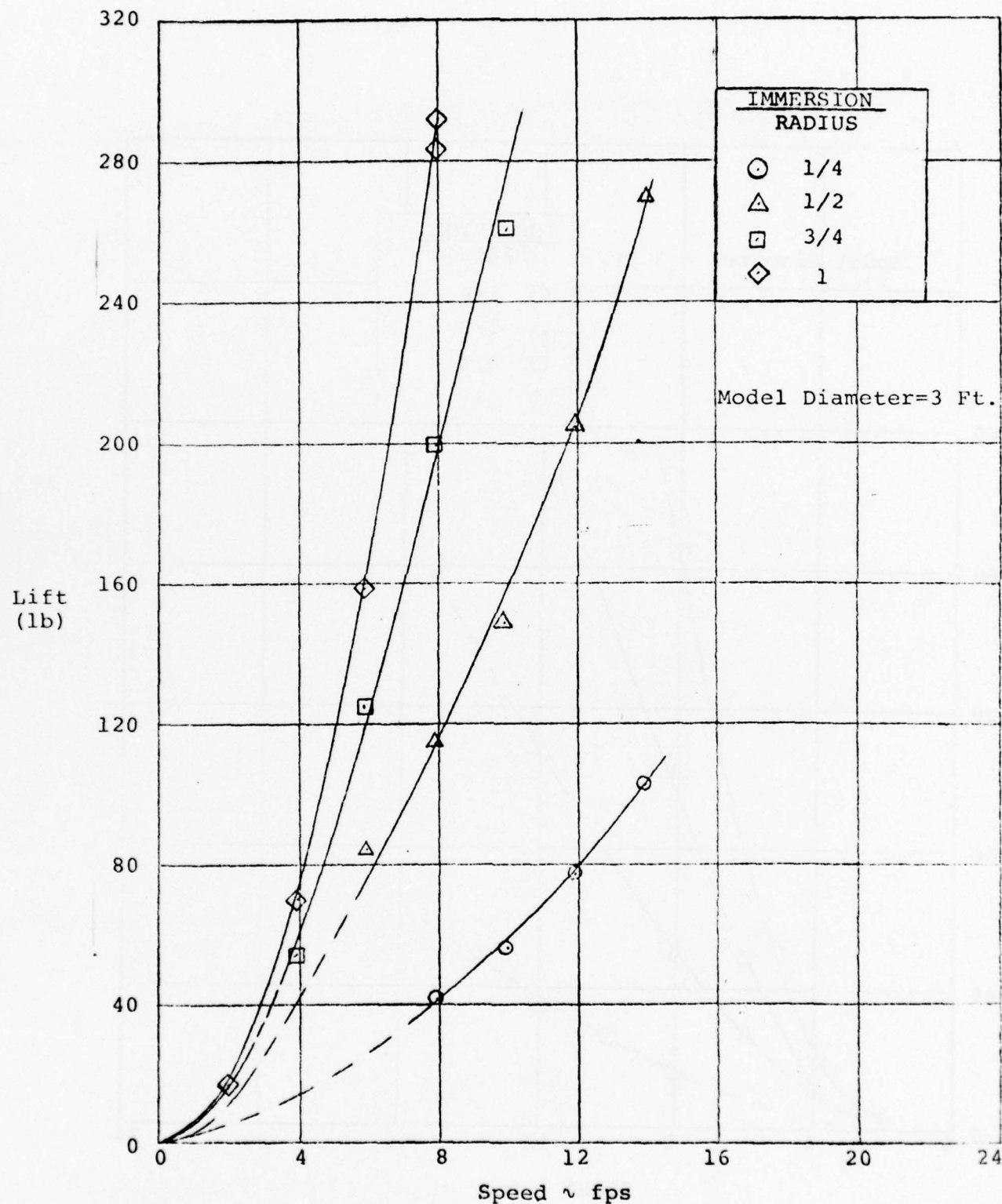


Figure 6. Hydrodynamic Lift for a Hemispherical Buoy

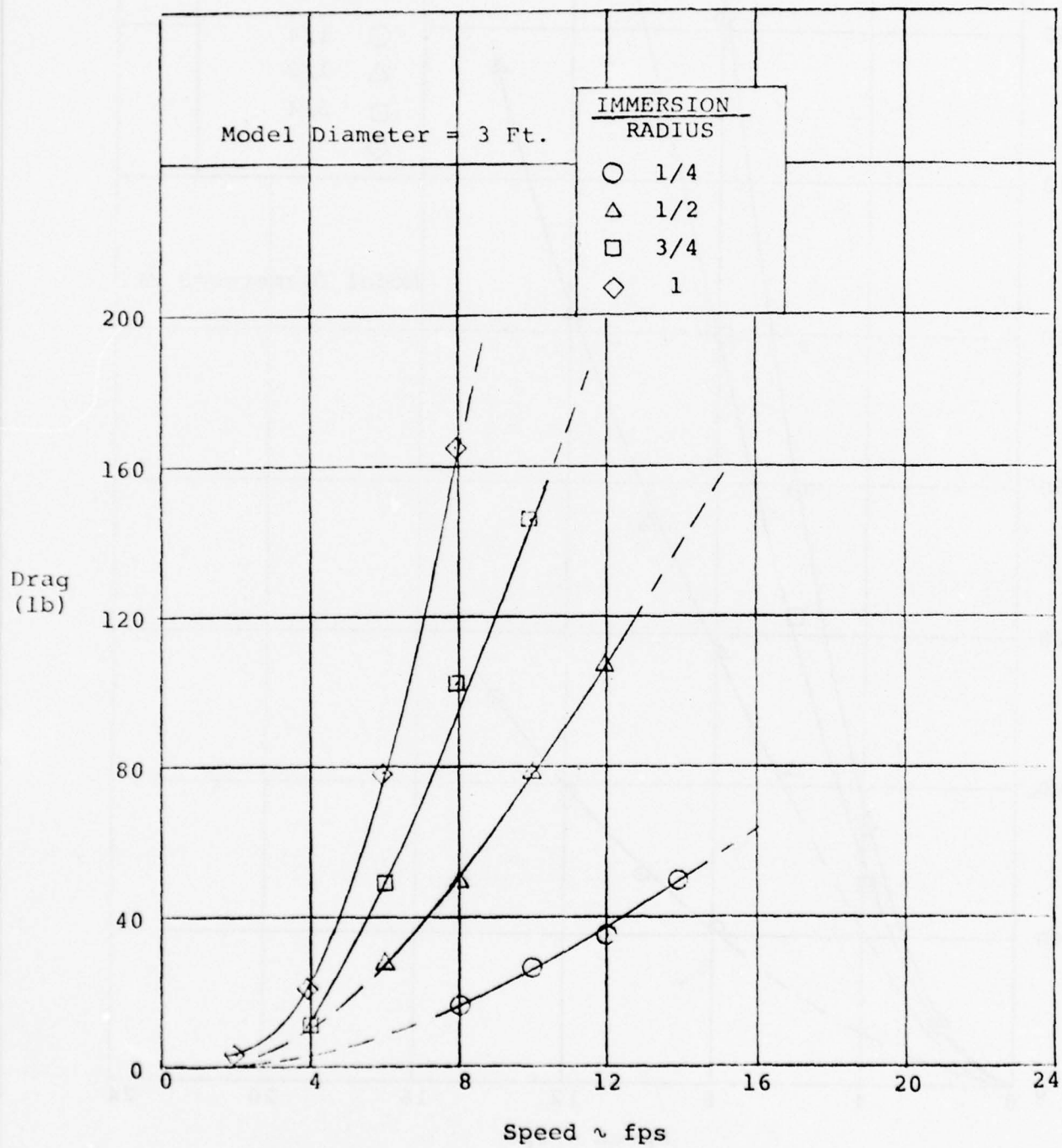


Figure 7. Hydrodynamic Drag for a Hemispherical Buoy

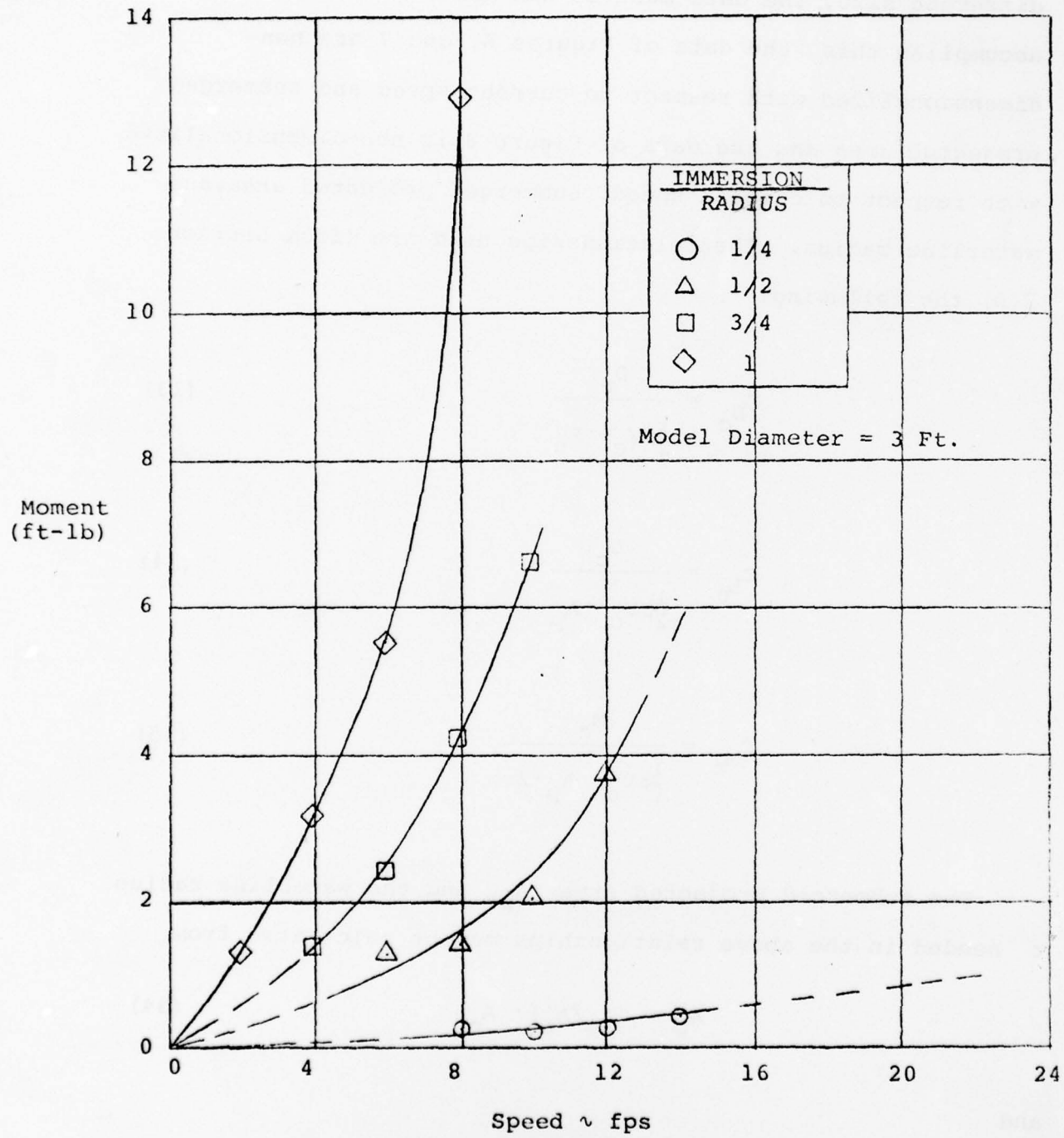


Figure 8. Hydrodynamic Pitching Moment for a Hemispherical Buoy

As discussed earlier, for these data to be useful in predicting the performance of other similarly shaped buoys of different size, the data must be non-dimensionalized. To accomplish this, the data of Figures 6 and 7 are non-dimensionalized with respect to current speed and submerged projected area and the data of Figure 8 is non-dimensionalized with respect to current speed, submerged projected area, and waterline radius. The relationships used are (from Section 2.0) the following:

$$C_{D_C} = \frac{D_C}{\frac{1}{2}\rho V_C^2 \cdot A_p} \quad (13)$$

$$C_{L_C} = \frac{L_C}{\frac{1}{2}\rho V_C^2 \cdot A_p} \quad (14)$$

$$C_{M_C} = \frac{M_C}{\frac{1}{2}\rho V_C^2 \cdot A_p \cdot 2r} \quad (15)$$

The submerged projected area A_p and the waterline radius r needed in the above relationships may be calculated from

$$A_p = (A_p/A_o) \cdot A_o \quad (34)$$

and

$$r = (r/R) \cdot R \quad (35)$$

where (A_p/A_o) and (r/R) are only functions of the relative buoy immersion d/R and may be obtained from Equations (29) and (33) of Section 3.0 or directly from Figure 3. Knowing the basic geometric characteristics of the test model, i.e., its radius, its semicircular projected area A_o can also be calculated (cf., Figure 3).

To properly scale these coefficients, Froude number dependence must be taken into account. Using the recorded current speeds for each test and the value of the waterline radius as determined from Equation (35) above, the Froude number for each test data is defined by

$$F_r = \frac{V_c}{\sqrt{2gr}} \quad (36)$$

(note: it is appropriate to use the waterline radius in defining the Froude number in this instance even though it is not a fixed dimension of the buoy since it is only the geometry of the buoy at and under the waterline which can actually influence its hydrodynamic characteristics.)

The data of Figures 6, 7, and 8 are nondimensionalized using Equations (13), (14), (15), (34), and (35) and may be plotted against the Froude number obtained from Equation (36). The results of this data reduction are presented as Figures 9, 10, and 11 where the hydrodynamic lift, drag, and pitching moment coefficients are shown, respectively, plotted against Froude number with the buoy relative immersion d/R as the parameter of the curves.

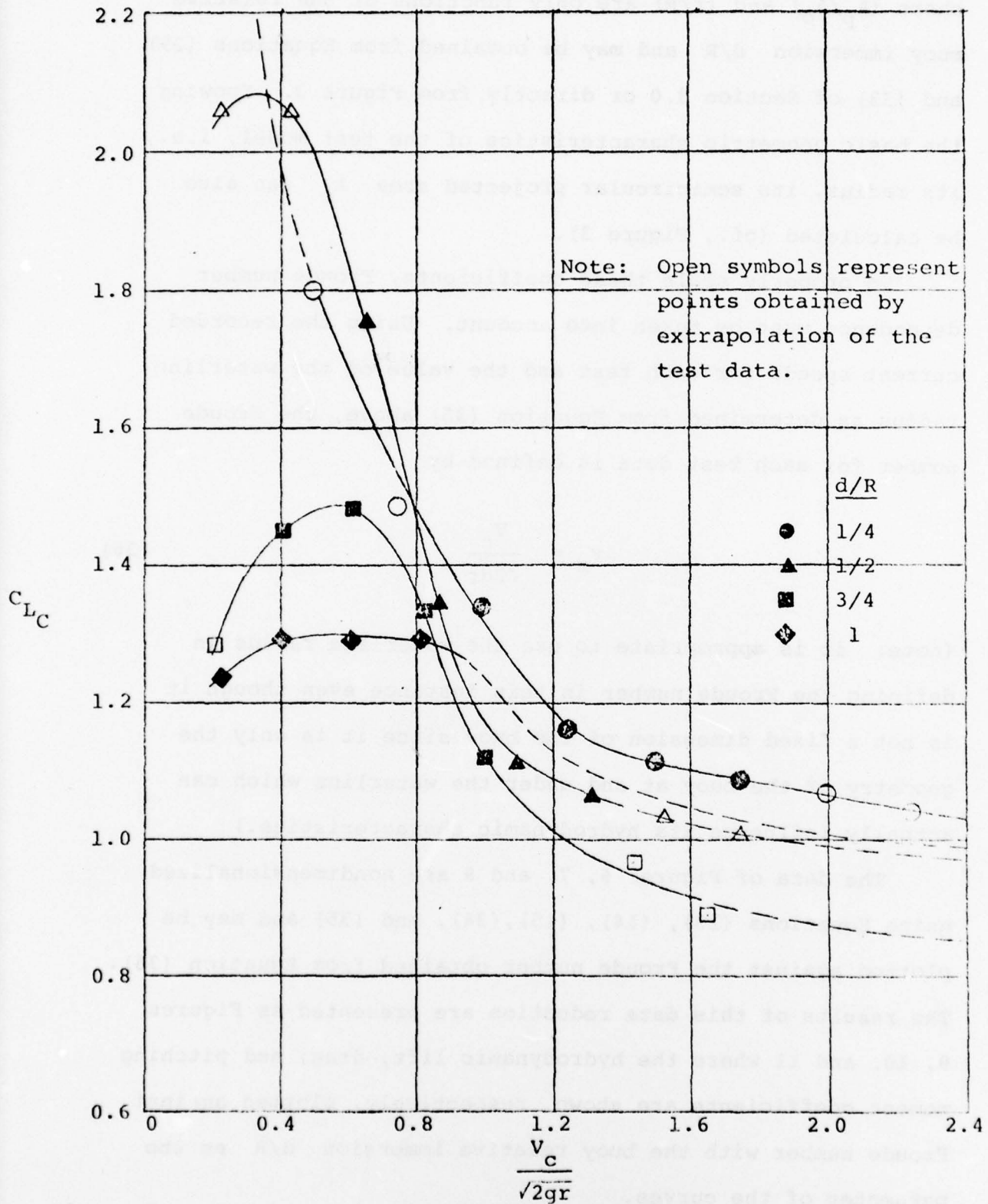


Figure 9. Hydrodynamic Lift Coefficient for a Hemispherical Buoy

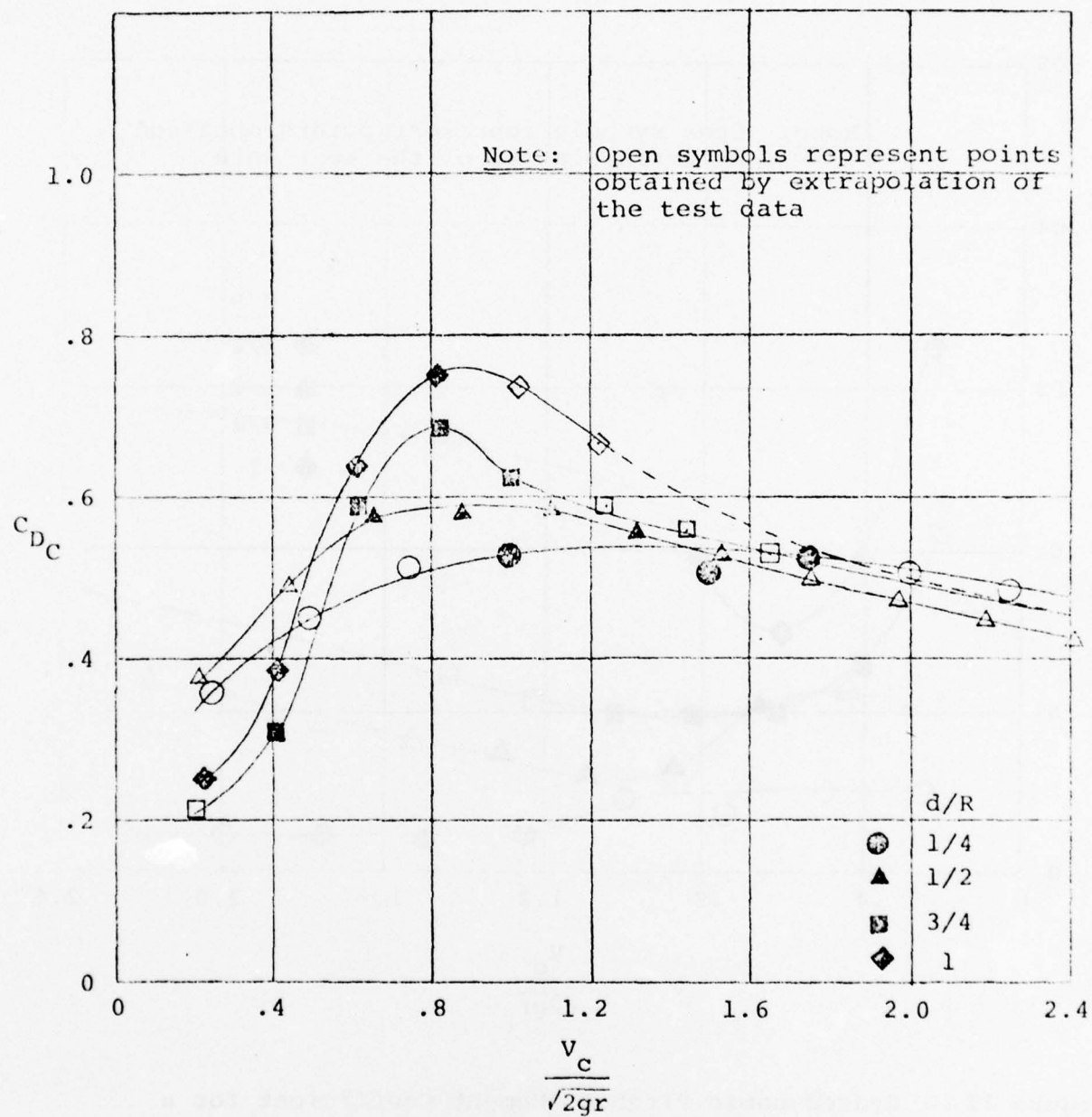


Figure 10. Hydrodynamic Drag Coefficient for a Hemispherical Buoy

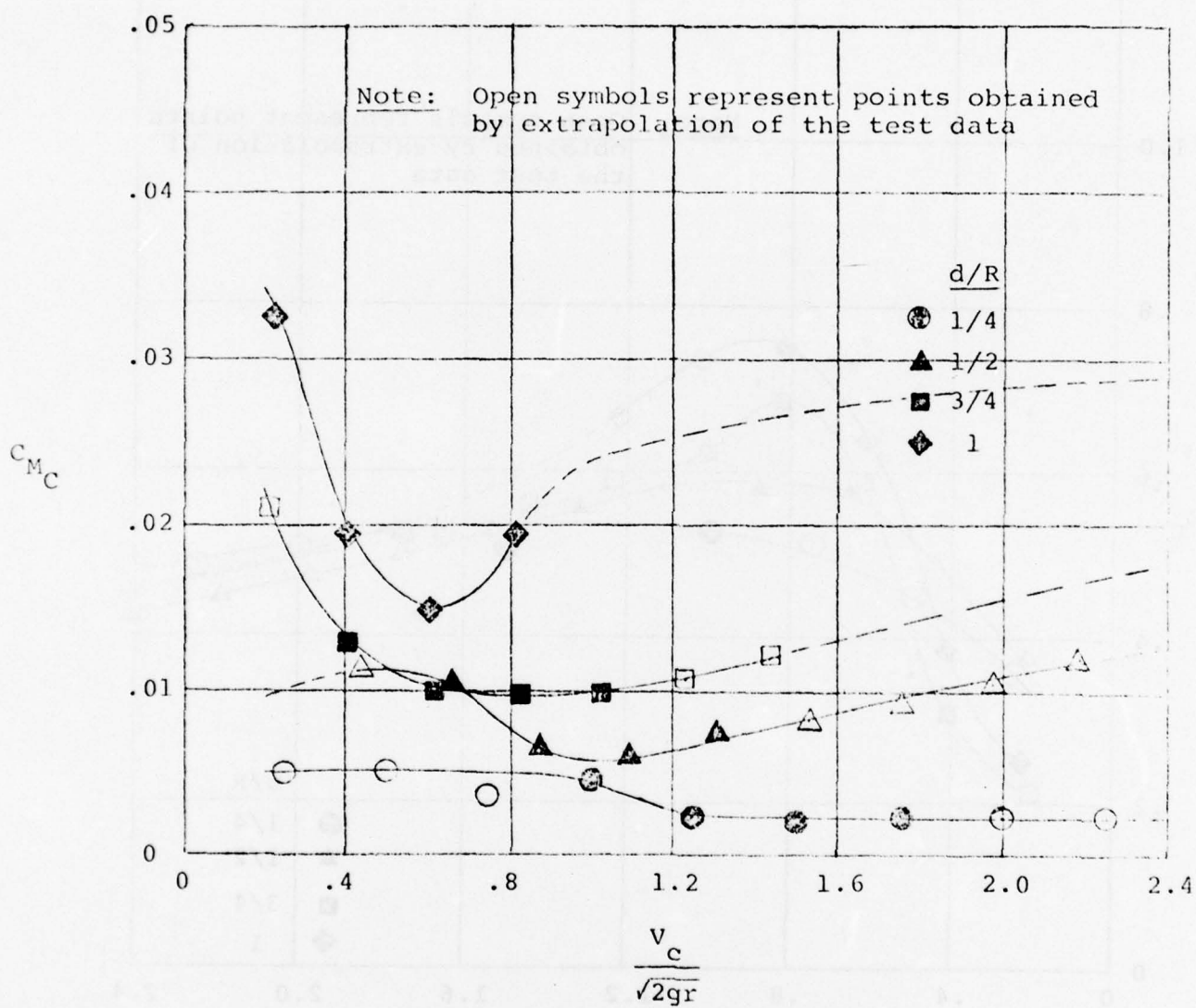


Figure 11. Hydrodynamic Pitching Moment Coefficient for a Hemispherical Buoy

5.0 VALIDATION OF THE MATHEMATICAL MODEL

5.1 Introduction

The analysis presented in Section 2.0 of this report developed a mathematical model for predicting the performance of a moored hemispherical buoy in a fast current. Two separate tasks were undertaken to validate this model. In the first, a computer program based upon the model was developed. The program enables the cable static equations to be solved numerically for a wide variety of buoy sizes, cable characteristics, cable-buoy attachment conditions, water depths, and current speeds. The program, although written for the specific geometry of a hemispherical shaped buoy, was modelled after the buoy-cable dynamics program developed by Oceanics, Inc. and described in [10].

Work on the development of the fast water buoy computer program, described in detail in the program manual which was written for it [11], was started early in this study program. The objective was to use this predictive tool not only to validate the mathematical model, but also to survey the conditions proposed for a series of validation towing tank tests so as to insure that the high current speeds proposed for these tests would not jeopardize the survival of the test model.

The second task undertaken to validate the mathematical model was a series of towing tank tests conducted in January 1976 at the Danish Ship Research Laboratory. The tests were designed to simulate the situation of this type of buoy placed in

relatively shallow, calm water, i.e., a 10' depth, in a high speed uniform current environment. The subsections which follow describe the test program in detail.

5.2 The Characteristics of the Test Model

The model used for the validation test program was essentially the same model used for the hydrodynamic force and moment tests described in Section 3.0. The model was made of wood, varnished on the outside and reinforced with fiberglass and polyester on the inside. It was provided with a deck with a hatch giving easy access to the internal ballast and facilitating changes of location of the eyebolt to which the towing cable was shackled. In order to provide a good reference for the measurements of pitch angle, a 4'6" aluminum pole was erected on the model with its axis coinciding with the symmetry axis of the model (the z-axis).

Photo grid markings were painted on the model in order to enable changes of draft during towing to be estimated. The model was ballasted so as to obtain the desired weight and stability conditions. The only other difference between this model and the version of it used during the hydrodynamic force and moments tests was the presence in those tests of a deck and a spray guard. Figure 12 is a sketch of the actual model used in this test series showing the photogrid and a typical cable attachment location. Figure 13 is an actual photo of the model in the workshop.

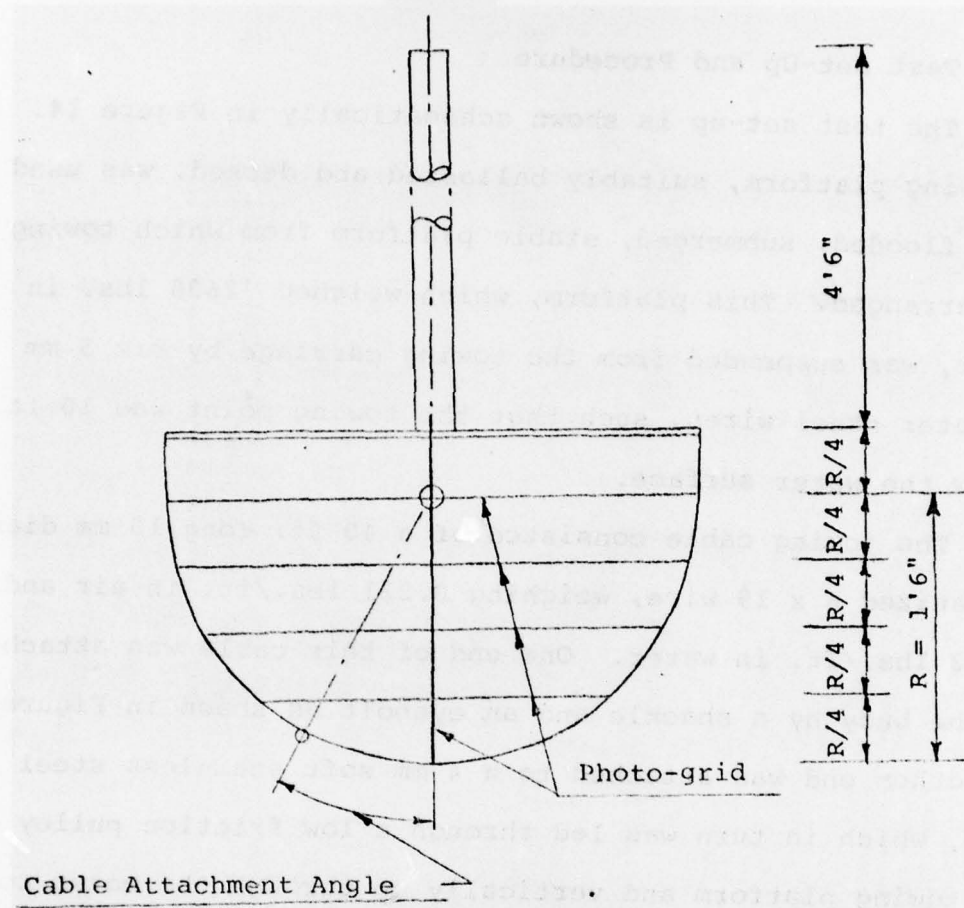


Figure 12. Model Outline

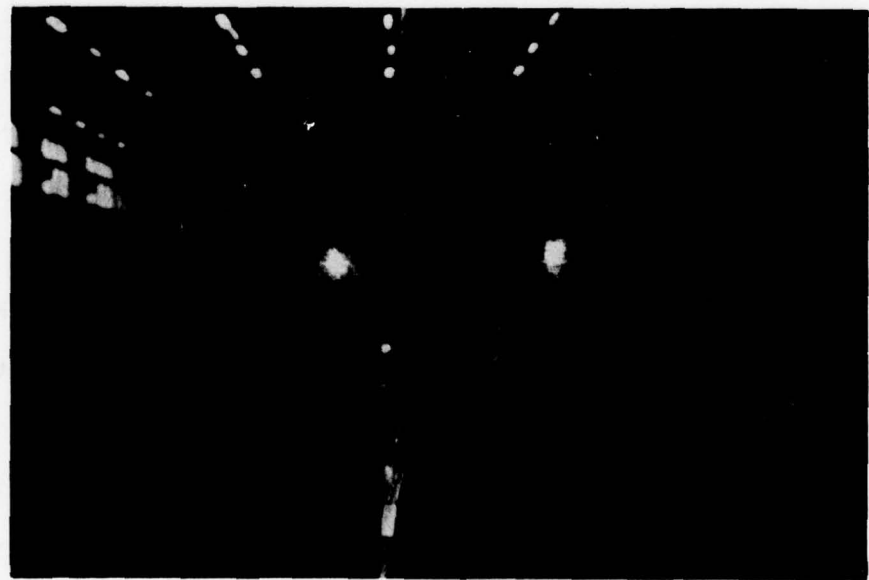


Figure 13. Photo of Model in Workshop

5.3 Test Set-Up and Procedure

The test set-up is shown schematically in Figure 14.

A towing platform, suitably ballasted and decked, was used as a flooded, submerged, stable platform from which towing was arranged. This platform, which weighed 2600 lbs. in water, was suspended from the towing carriage by six 5 mm diameter steel wires, such that the towing point was 10 ft. below the water surface.

The towing cable consisted of a 40 ft. long 10 mm diameter galvanized 6 x 19 wire, weighing 0.221 lbs./ft. in air and 0.183 lbs./ft. in water. One end of this cable was attached to the buoy by a shackle and an eyebolt as shown in Figure 15. The other end was attached to a 4 mm soft stainless steel wire, which in turn was led through a low friction pulley on the towing platform and vertically up through the water to a dynamometer on the towing carriage.

Before the actual tests were begun, a few runs were performed without the buoy in order to check the stability of the submerged towing platform at various speeds. From visual inspection the platform proved to be completely stable at all speeds and no surface waves induced by the submerged platform could be seen.

During the actual test runs motion pictures were taken of the buoy by means of a camera situated on a photo platform on the after end of the towing carriage (see Figure 14). In addition, during each run a snap-shot was taken from a fixed point in the tank, the photo being taken at approximately

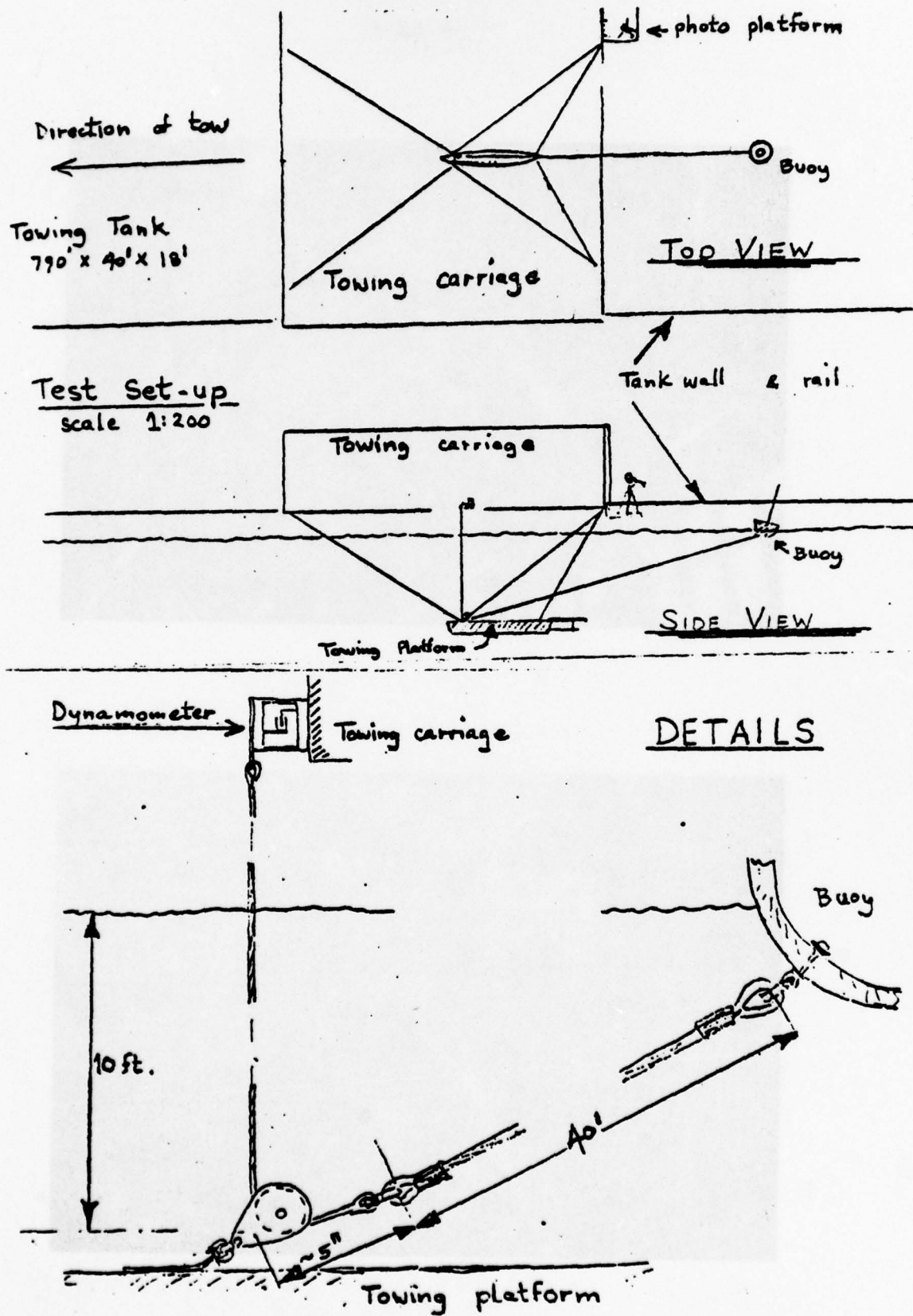


Figure 14. Test Set-up

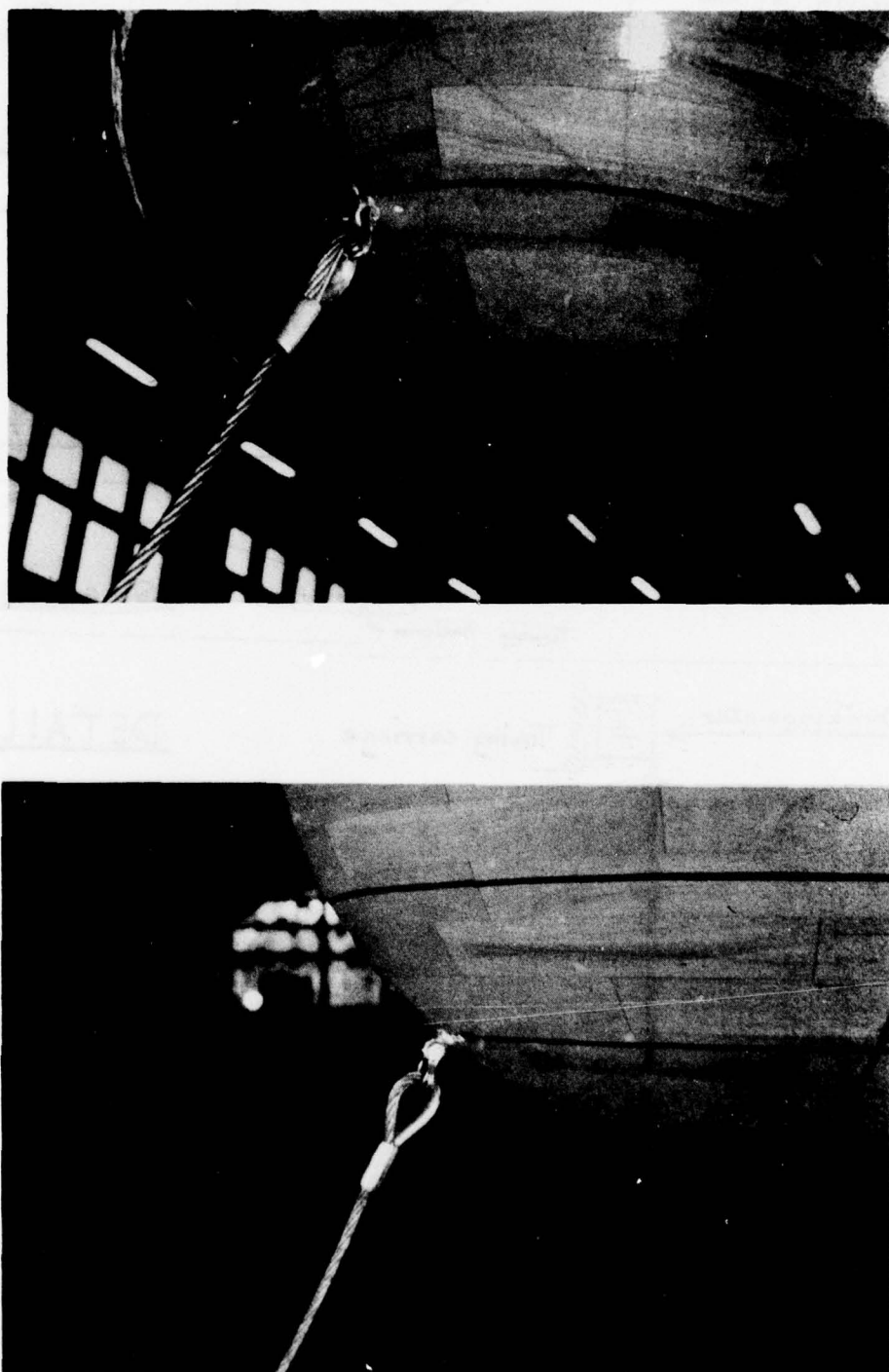


Figure 15. Photos Showing Details of Cable Attachment

right angles to the direction of motion of the buoy. The pitch angle of the buoy was measured from the still photographs using the far wall and rail of the tank and the aluminum pole on the buoy as references. An estimate of the draft of the buoy was also obtained from these photographs.

5.4 The Range of Test Conditions and Measurements Taken

A total of 11 test runs were made for various speeds, mooring attachment points (on buoy), and for two loading conditions. During each run, the towing speed and cable tensions were recorded. Table 2 below presents the matrix of cases tested along with the loading conditions, cable attachment angles, and towing (current) speeds used for each.

TABLE 2
MATRIX OF VALIDATION TEST RUNS

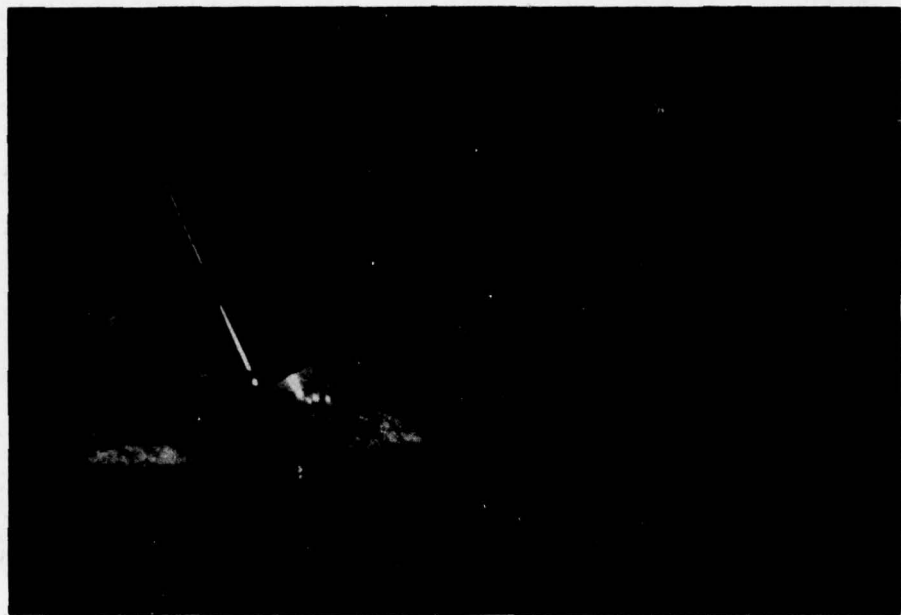
Run No.	Displacement lbs.	GM inches	Cable Attachment Angle (deg.)	Speed	
				ft./sec.	mph
1	100	5.0	25	6.00	4.09
2	100	5.0	25	8.00	5.45
3	100	5.0	40	8.00	5.45
4	100	5.0	40	6.00	4.09
5	100	5.0	60	8.00	5.45
6	100	5.0	60	6.01	4.10
7	70	4.6	60	8.00	5.45
8	70	4.6	60	6.00	4.09
9	70	4.6	60	7.00	4.77
10	70	4.6	40	8.00	5.45
11	70	4.6	40	8.96	6.10

5.5 Results and Comparison with Numerical Predictions

Prior to the actual towing tank test runs a series of computer program runs were made with the Fast Water Buoy program for the same set of conditions under which the tank tests were to be conducted. Table 3 below presents the results of both the experimental runs and the computer simulations. The cable tensions recorded during the towing tank runs (and listed below) are those that were measured and correspond to the cable anchoring point on the towing platform simulating the bottom. In addition to these tensions, Table 3 also includes the pitch angle observed from the still photographs, which are shown as Figures 16(a) - 16(g). The results from the computer simulations present the equilibrium buoy trim angle and the cable tension at the anchor, which also happens to be the maximum cable tension in the system.

TABLE 3
TEST RESULTS AND PROGRAM PREDICTIONS

Run No.	Experimentally Determined Cable tension lbs.	Results from Computer Simulation Cable tension lbs.	Experimentally Determined Pitch angle, bow up deg.	Results from Computer Simulation Pitch angle, bow up deg.
1	40.6	46.2	26	28.7
2	187.8	170.8	43	45.0
3	193.7	171.1	29.5	31.7
4	43.2	46.3	16	19.0
5	192.9	171.5	10.5	14.3
6	43.2	46.4	4	6.1
7	159.9	139.6	11	13.5
8	33.5	39.7	2	5.8
9	78.7	72.5	8	9.5
10	163.7	129.5	30	30.5
11	221.6	209.6	31	41.7



Run No. 1 Speed 6 Feet Per Second
Cable Attachment Angle 25 Deg. Pitch Angle 26 Deg.

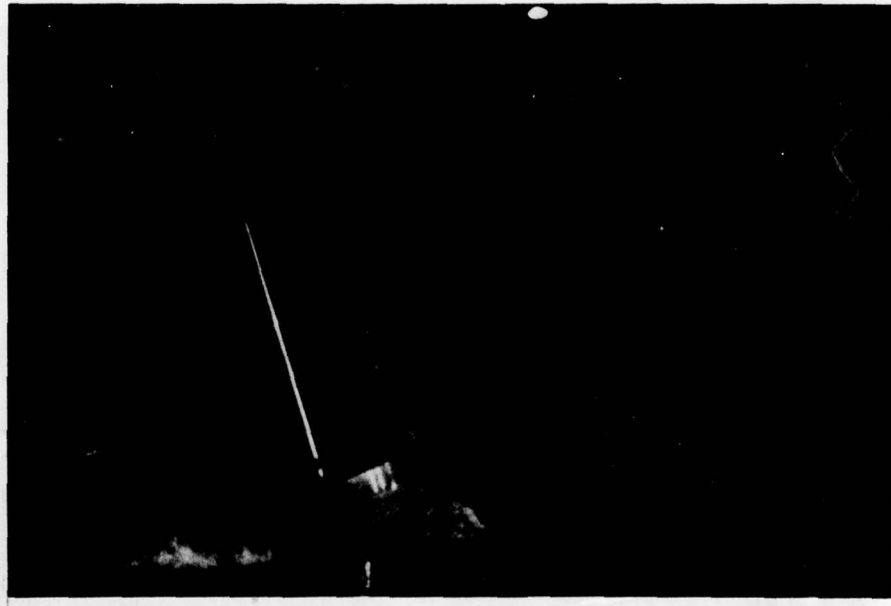


Run No. 2 Speed 8 Feet Per Second
Cable Attachment Angle 25 Deg. Pitch angle 43 Deg.

Figures 16(a)-16(g). Still-Photographs Taken to Determine Pitch Attitude of Buoy During Validation Tests.

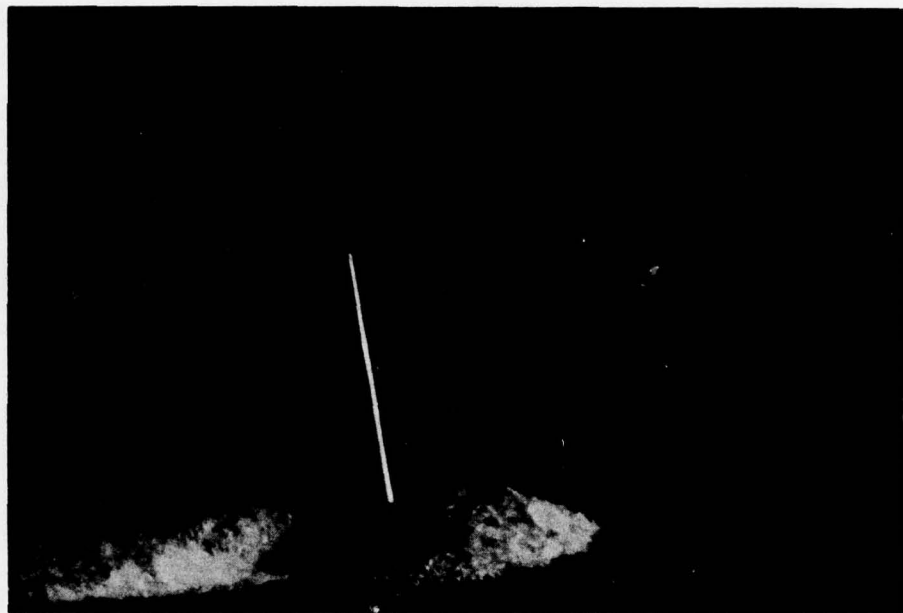


Run No. 3 Speed 8 Feet Per Second
Cable Attachment Angle 40 Deg. Pitch Angle 29 1/2 Deg.

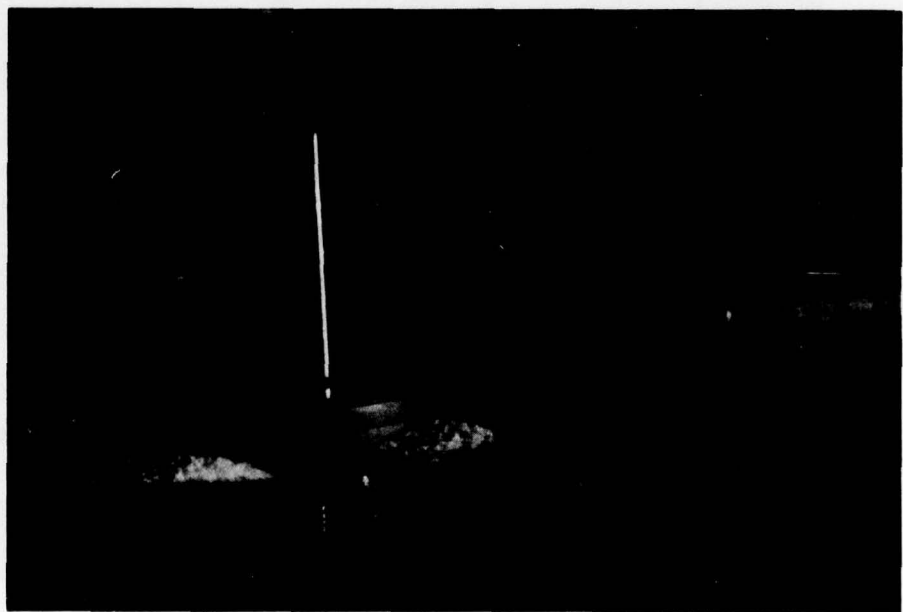


Run No. 4 Speed 6 Feet Per Second
Cable Attachment Angle 40 Deg. Pitch Angle 16 Deg.

Figure 16(b)

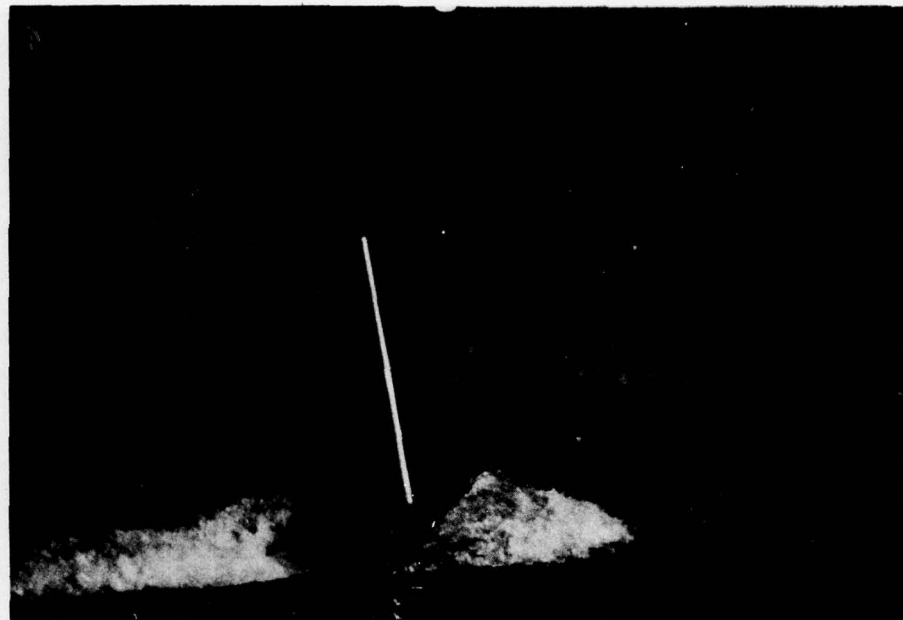


Run No. 5 Speed 8 Feet Per Second
Cable Attachment Angle 60 Deg. Pitch Angle 10 1/2 Deg.

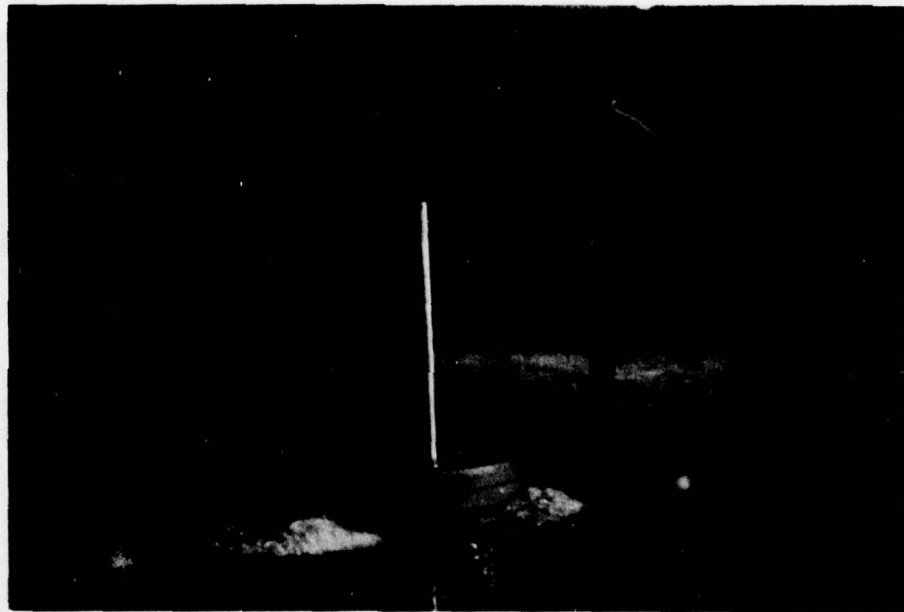


Run No. 6 Speed 6.01 Feet Per Second
Cable Attachment Angle 60 Deg. Pitch Angle 4 Deg.

Figure 16(c)

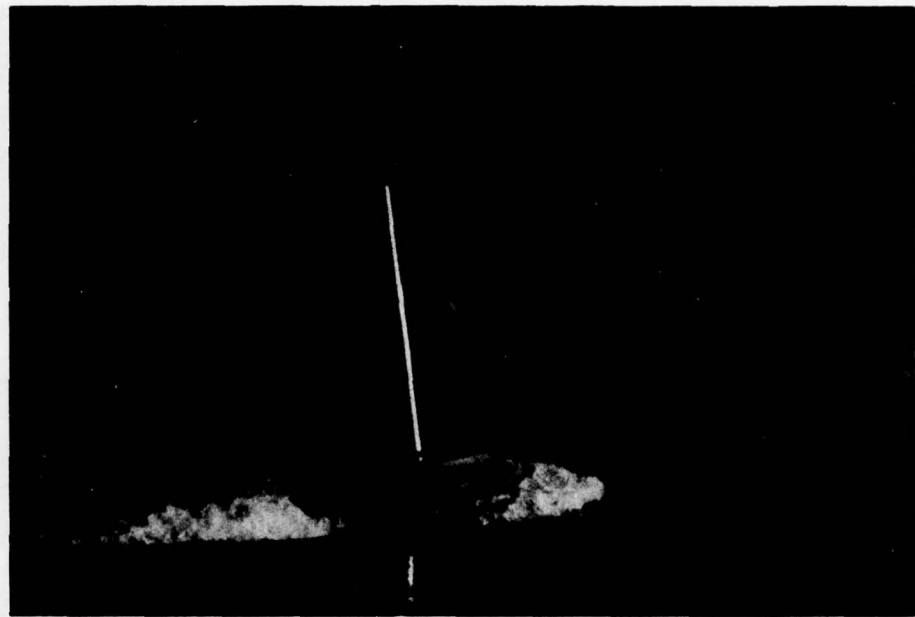


Run No. 7 Speed 8 Feet Per Second
Cable Attachment Angle 60 Deg. Pitch Angle 11 Deg.



Run No. 8 Speed 6 Feet Per Second
Cable Attachment Angle 60 Deg. Pitch Angle 2 Deg.

Figure 16(d)



Run No. 9 Speed 7 Feet Per Second
Cable Attachment Angle 60 Deg. Pitch Angle 8 Deg.



Run No. 10 Speed 8 Feet Per Second
Cable Attachment Angle 40 Deg. Pitch Angle 30 Deg.

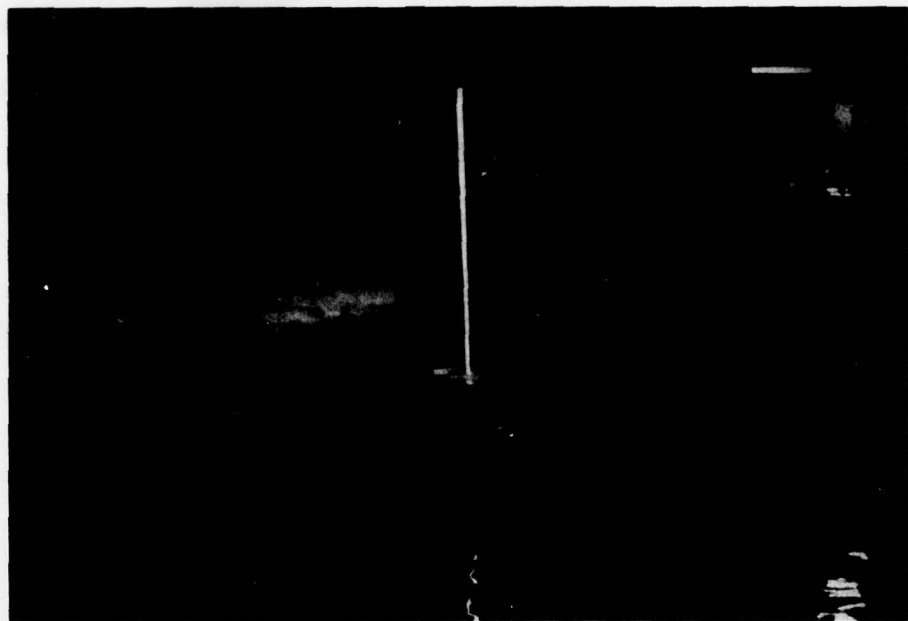


Run No. 11 Speed 8.96 Feet Per Second
Cable Attachment Angle 40 Deg. Pitch Angle 31 Deg.

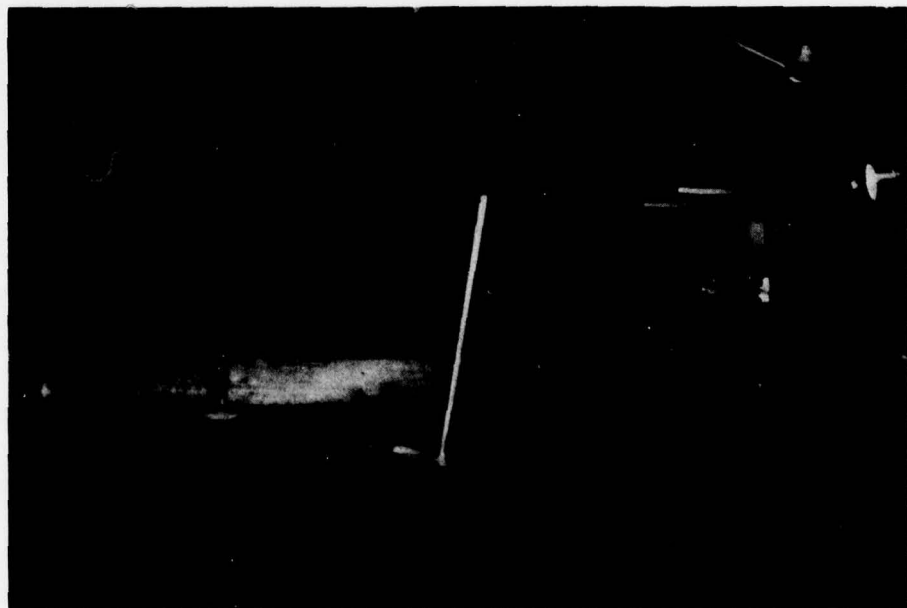


Same as Case Above. Stern Quarter View.

Figure 16(f)



Zero Speed Without Towing Cable



Zero Speed With Towing Cable

These results show an average percentage difference between the experimentally determined values of the tension and the computer program-generated-values of the order of 11%. It is also worthwhile to note that the buoy proved to be quite stable during towing with only small damped oscillations occurring, which were probably induced during the acceleration period and by small waves present in the tank from previous runs.

6.0 PARAMETRIC STUDY RESULTS

6.1 Introduction - Parameter Selection

In order to determine the optimum mooring attachment point for a hemispherical buoy in a high speed current, the design tool which had been developed was systematically exercised. The ranges of investigation of some of the buoy, cable, and environmental parameters were reexamined in the light of the results obtained from the validation tests. With the guidance of Coast Guard Research and Development personnel the parameter ranges presented in Table 4 below served as the limits of the parametric study.

TABLE 4

REVISED HEMISPHERICAL BUOY - CABLE SYSTEM PARAMETERS

Buoy Hull Diameters, d_B	-	3 - 6 ft.
Buoy Weights, W_B	-	50 - 350 lbs.
Buoy Metacentric Heights, GM	-	2 - 12 inches
Cable Lengths, l_c	-	40 - 100 ft.
Water Depths, h	-	7 - 40 ft.
River Current Speeds, V_c	-	3 - 11 mph
Cable Diameters, d_c	-	1/8 - 1/2 inch

The complete ranges of all of the above were also not appropriate for the cases to be investigated. Again, with Coast Guard guidance, the following variations were considered.

TABLE 5
APPROPRIATE PARAMETER COMBINATIONS

Buoy Diameter (ft.)	Buoy Weight (lbs)	Metacentric Height (in.)
3.0	50. - 80.	2. - 5.
4.0	70. - 140.	4. - 8.
5.0	120. - 240.	5. - 10.
6.0	220. - 350.	6. - 12.

Constraining Cable Length (ft.)	Water Depth (ft.)	Current Speed (mph)
40. - 100.	7. - 15.	3. - 5.
50. - 100.	16. - 20.	3. - 7.
75. - 100.	21. - 30.	3. - 9.
100.	31. - 40.	3. - 11.

Cable Diameters (in.): 1/8 - 1/2

Even the above ranges are rather large. Hence, in order to get as complete a sampling of parameters as possible and still remain within a realistic number of cases to be run, the following cases were agreed upon:

- (A) Each of the 4 buoy diameters in Table 5 would be examined.
- (B) Each diameter would be examined for the 2 extremes in weight variation for each.
- (C) Each diameter would be examined for the 2 extremes in metacentric height for each.
- (D) 4 current speeds would be considered. The upper extremes shown in Table 5 would be used.
- (E) For each current speed a single depth was selected using the lower extreme for the lowest current speed, the upper extreme for the highest current speed, and mid values for the remaining two current speeds, as shown below in Table 6.
- (F) For each current speed, two cable lengths would be considered. These would be the extremes given in Table 5 for each current speed.

TABLE 6

CURRENT SPEED - DEPTH - CABLE LENGTH

Current Speed (mph)	Water Depth (ft.)	Cable Length (ft.)
5.	7.0	40., 100.
7.	18.0	50., 100.
9.	25.0	75., 100.
11.	40.0	100.

For each of these cases, 3 cable attachment angles; 10° , 35° , and 60° were to be considered, with attachment at the maximum radius.

The effect of cable diameter was to be studied by selecting 1 buoy diameter, weight, and metacentric height combination and then changing the cable diameter from $1/2"$ (at which all other cases previously mentioned were to be run) to $1/8"$ for two of the current speeds under investigation.

One of the other specific objectives of the study, i.e., to determine the sensitivity of the results obtained to variations in drag due to debris accumulation, was to be accomplished by determining the effect of an attachment drag at the buoy-cable attachment point. The debris was assumed to be neutrally buoyant and the drag produced by it was assumed to be some percentage of the drag on the cable itself. This auxiliary portion of the study totalled 8 cases. Two drag values were to be used along with 2 buoy diameters (3' and 6') and 2 current speeds (5 and 7 mph).

A few additional cases were run to check the effect of cable drag coefficient on buoy-cable system performance. Examination of the literature, [12] and [13], indicated that cable drag coefficients can be from 15 to 60 percent higher than the level used in these studies depending upon how the cable is constructed. Two additional cases were run with cable drag coefficients increased by the above percentages for a 4 ft. diameter buoy in a 7 mph current.

The last additional cases to be run were selected to determine the influence of the elastic properties of the

cable on system performance. The parametric study cases mentioned above were all run with a cable assumed to be made from an inelastic material or one with a very high elastic modulus. The additional cases mentioned here were run with an elastic modulus for nylon assuming the cable to be circular in cross section with a diameter of 1/2 inch. Runs were made for a 6 ft. diameter buoy at current speeds of 5, 7 and 9 mph.

6.2 Discussion of the Results

One of the most important objectives of the study was to determine what cable attachment angles would result in minimizing the buoy trim angle for any given current environment. The results appear to be very clear and are illustrated in Figure 17.

Equilibrium trim angle, θ , is plotted against cable attachment angle, α , for a 6 ft. diameter buoy in current speeds of 5, 7, and 9 mph. These results show a steady reduction in pitch trim with increasing attachment angle for all current speeds for which solutions were obtained. The 6 ft. diameter buoy was chosen to be representative because it was able to survive in the higher current environments whereas the smaller diameter buoys were not. However, whenever equilibrium for the smaller buoys was achieved, i.e., they did not sink or their trim angles did not go to 90° , increasing the attachment angle resulted in lower buoy trim angles.

The other single universal influence which resulted in reduced buoy trim was the effect of increasing the metacentric height. Figure 18, which presents a plot of equilibrium trim angle against metacentric height for different buoy diameters and the range of attachment angles considered illustrates this. The absolute reduction in trim is more pronounced at

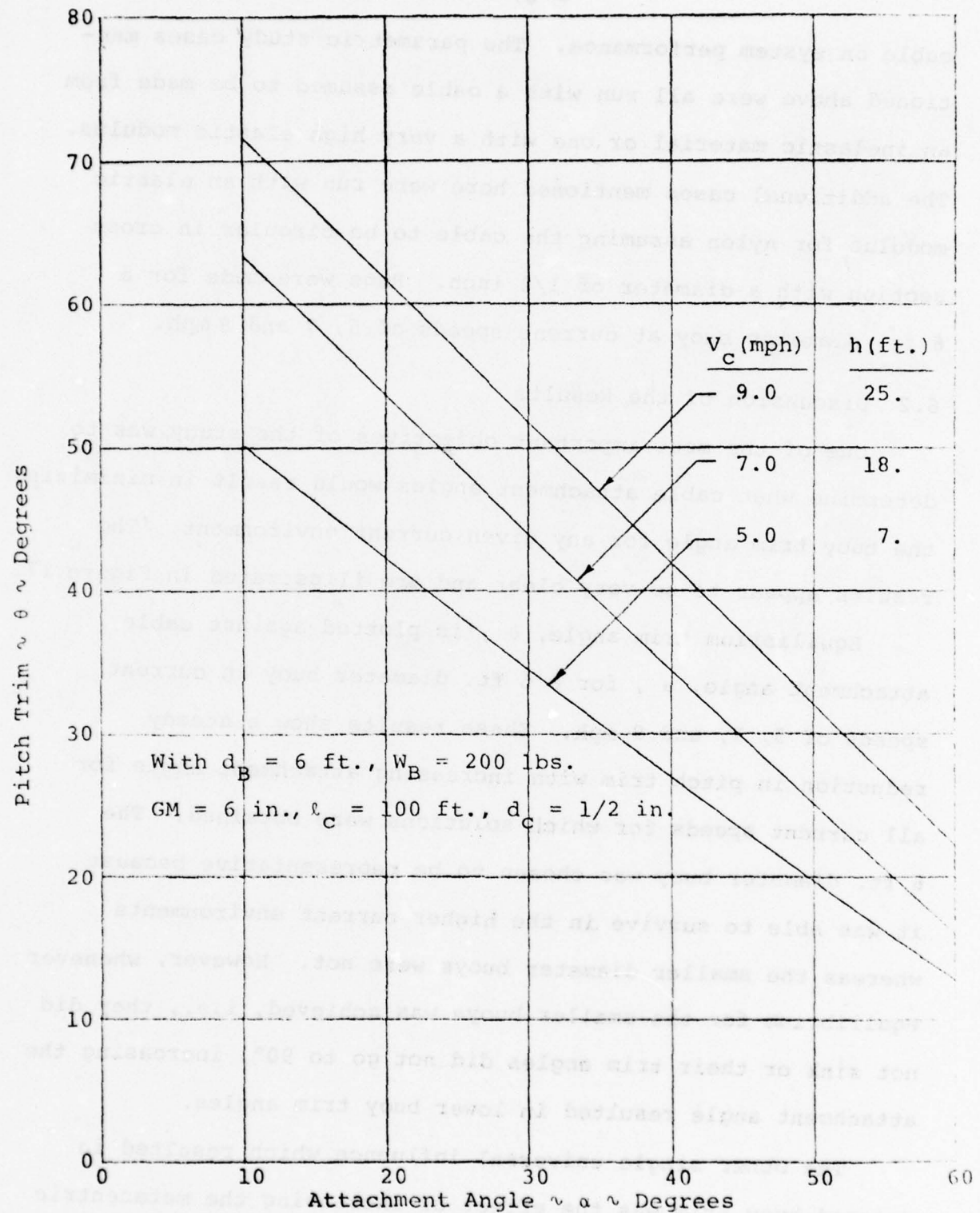


Figure 17. Trim vs. Attachment Angle for Various Current Speeds

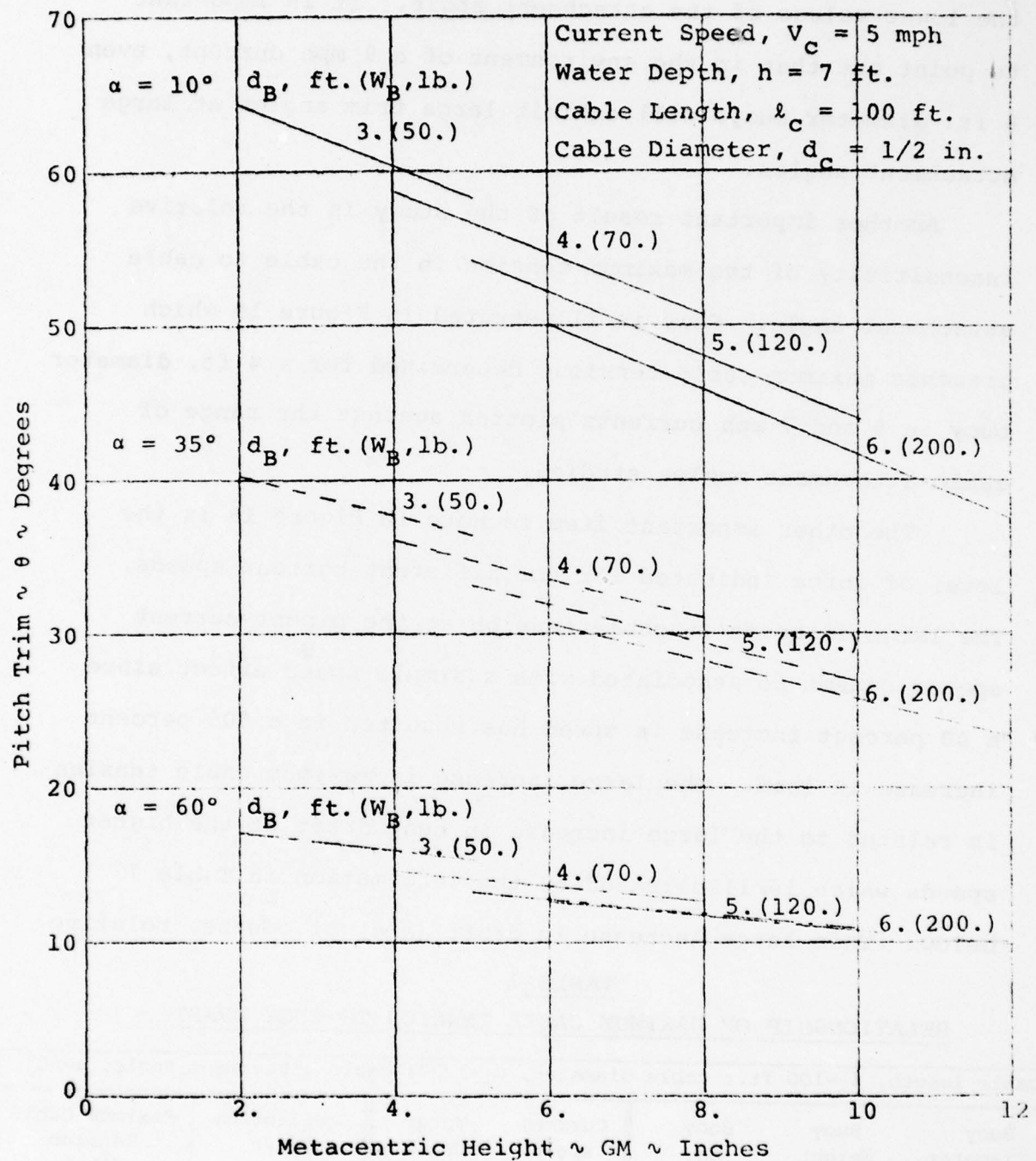


Figure 18. Trim vs. Metacentric Height For Various Buoy Diameters

the lower values of the attachment angle. It is important to point out that in the environment of a 9 mph current, even 6 ft. diameter buoys will exhibit large trim angles at large attachment angles.

Another important result of the study is the relative insensitivity of the maximum tension in the cable to cable attachment angle. This is illustrated in Figure 19 which presents maximum cable tensions determined for a 4 ft. diameter buoy in 5 and 7 mph currents plotted against the range of cable attachment angles studied.

The other important item to note in Figure 19 is the level of force indicated for the different current speeds. The large increase in cable tension at the higher current speeds cannot be associated with a simple speed effect since a 40 percent increase in speed has resulted in a 500 percent increase in load. The large increase in maximum cable tension is related to the large increase in buoy draft at the higher speeds which is illustrated by the information in Table 7 below. This large increase in draft (and, of course, relative

TABLE 7
RELATIONSHIP OF MAXIMUM CABLE TENSION TO BUOY DRAFT

cable length, l_c = 100 ft.; cable diameter, d_c = 1/2"; cable attachment angle, α = 60°						
Buoy Diameter (ft.)	Buoy Weight (lb.)	Buoy GM (in.)	Current Speed (mph)	Water Depth (ft.)	Equilibrium Draft (ft.)	Maximum Cable Tension (lb.)
4.0	70.	4., 8.	5.0	7.	0.88	68.5
4.0	70.	4., 8.	7.0	18.	1.61	355.3
5.0	120.	5., 10.	5.0	7.	0.89	73.9
5.0	120.	5., 10.	7.0	18.	1.52	354.0

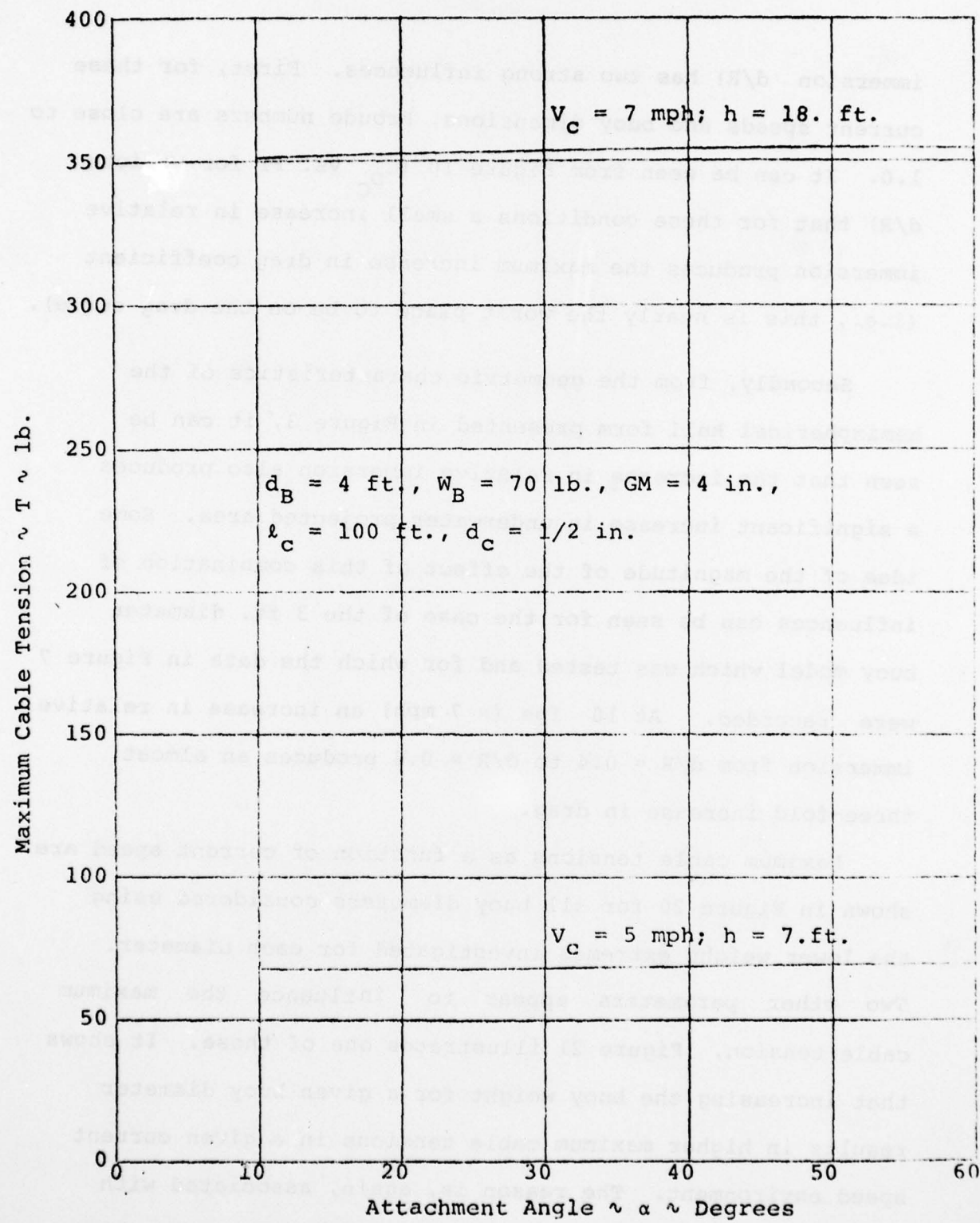


Figure 19. Maximum Cable Tension vs. Attachment Angle

immersion d/R) has two strong influences. First, for these current speeds and buoy dimensions, Froude numbers are close to 1.0. It can be seen from Figure 10 (C_{D_C} vs. Fr for various d/R) that for these conditions a small increase in relative immersion produces the maximum increase in drag coefficient (i.e., this is nearly the worst place to be on the drag curve).

Secondly, from the geometric characteristics of the hemispherical hull form presented in Figure 3, it can be seen that the increase in relative immersion also produces a significant increase in underwater projected area. Some idea of the magnitude of the effect of this combination of influences can be seen for the case of the 3 ft. diameter buoy model which was tested and for which the data in Figure 7 were recorded. At 10 fps (≈ 7 mph) an increase in relative immersion from $d/R = 0.4$ to $d/R = 0.8$ produces an almost three-fold increase in drag.

Maximum cable tensions as a function of current speed are shown in Figure 20 for all buoy diameters considered using the lower weight extremes investigated for each diameter. Two other parameters appear to influence the maximum cable tension. Figure 21 illustrates one of these. It shows that increasing the buoy weight for a given buoy diameter results in higher maximum cable tensions in a given current speed environment. The reason is, again, associated with the draft and hence relative immersion of the buoy as shown in Table 8 below. Increasing the buoy weight results in a

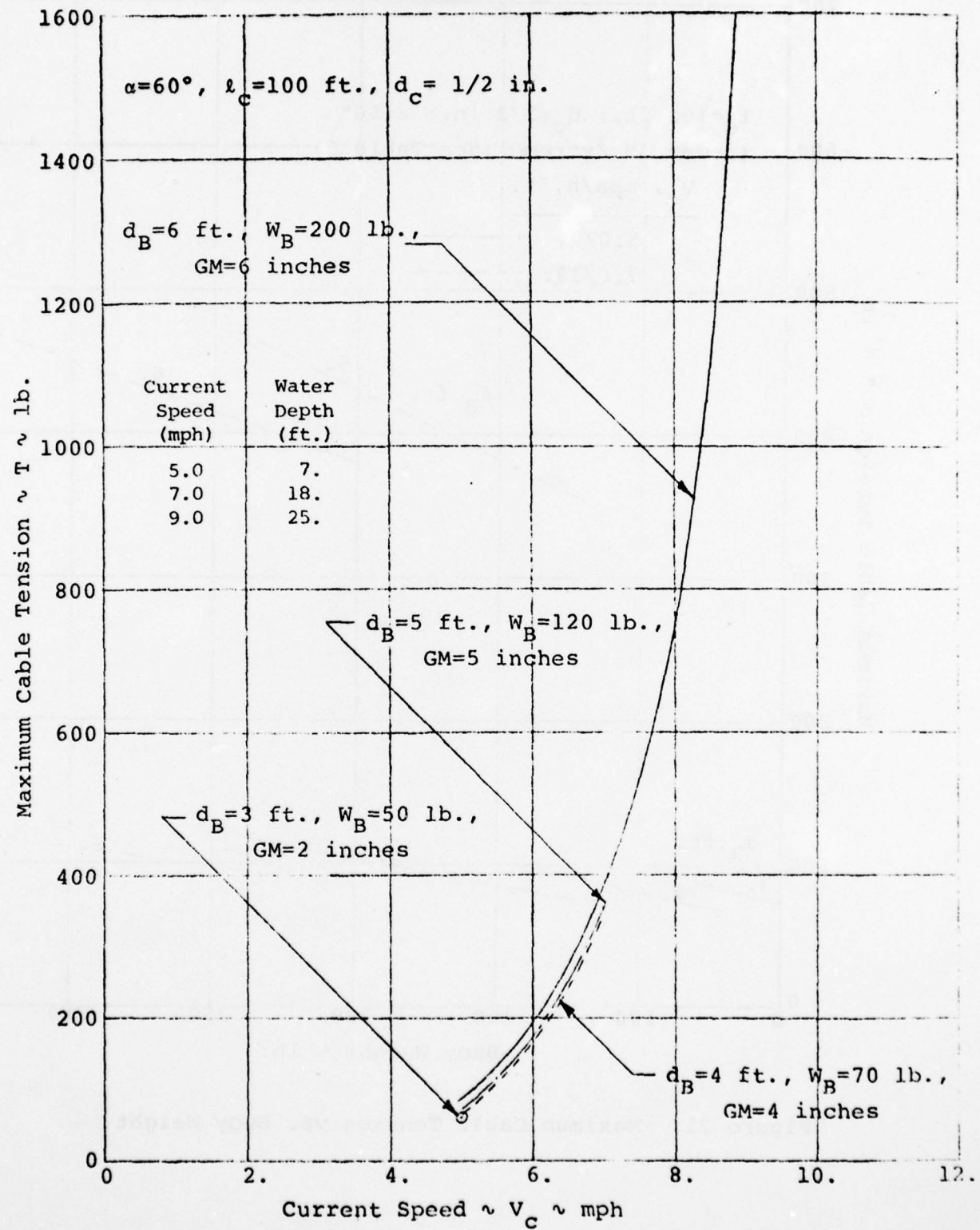


Figure 20. Maximum Cable Tension vs. Current Speed for Different Buoy Diameters

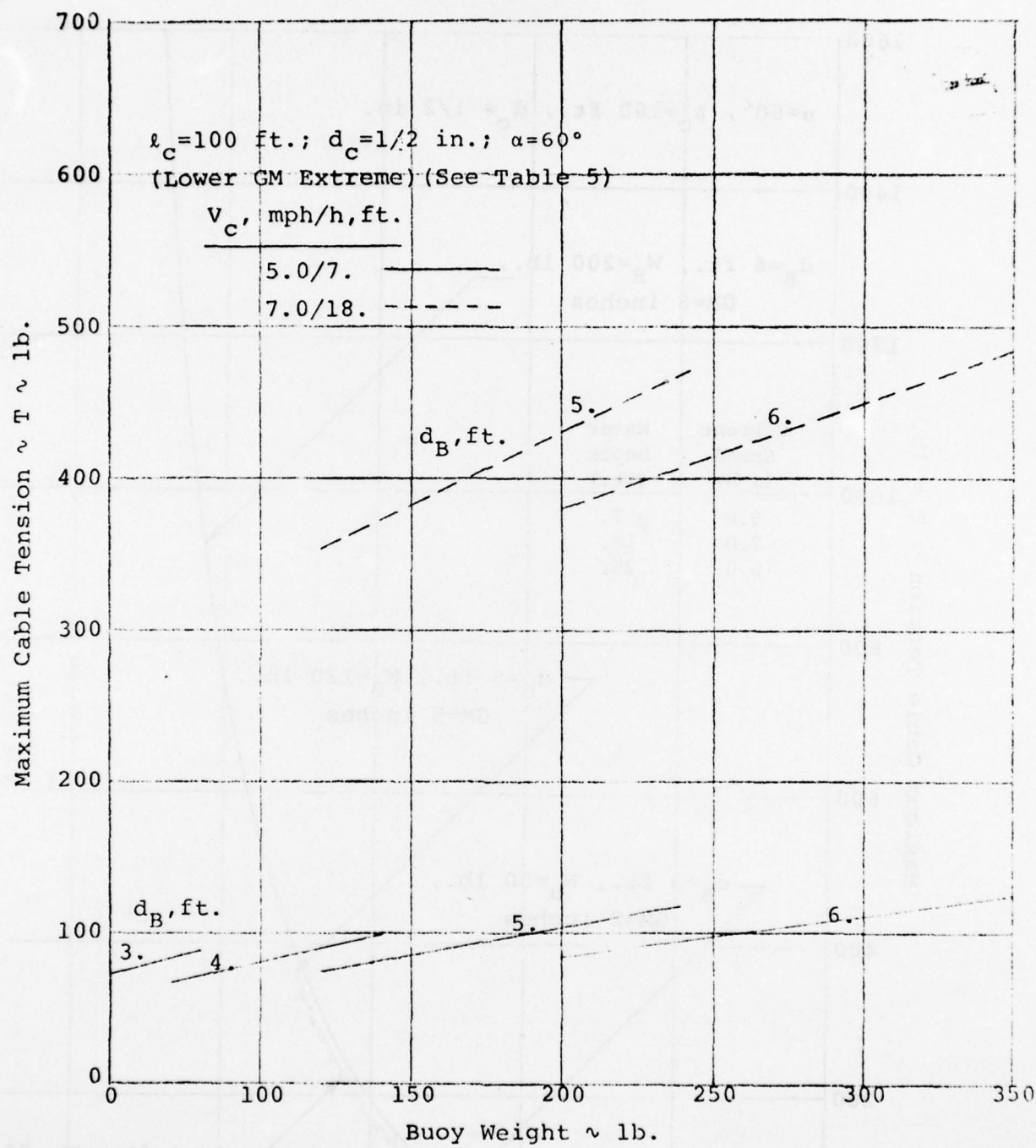


Figure 21. Maximum Cable Tension vs. Buoy Weight

TABLE 8

EFFECT OF INCREASED BUOY WEIGHT ON EQUILIBRIUM DRAFT AT FIXED
CURRENT SPEED

cable length, $l_c = 100$ ft.; cable diameter, $d_c = 1/2$ in.; cable attachment angle, $\alpha = 60^\circ$; current speed, $V_c = 5$ mph; water depth, $h = 7$. ft.			
Buoy Diameter (ft.)	Buoy Weight (lb.)	Metacentric Height (in.)	Equilibrium Draft (ft.)
4.0	70.	8.0	0.88
4.0	140.	8.0	1.12
5.0	120.	10.0	0.89
5.0	240.	10.0	1.21

slight increase in draft which increases cable tensions by 25 percent for the 3 ft. diameters and by 50 percent for the 4 ft. diameters.

Another parameter which appears to have an influence on the maximum cable tension is the effective scope of the mooring cable. Table 9 below shows the values used for the

TABLE 9

MOORING CABLE SCOPES

Current Speed (mph)	Water Depth (ft.)	Scopes	
		Shorter Cable	Longer Cable
5.	7.	5.7	14.3
7.	18.	2.8	5.6
9.	25.	3.0	4.0
11.	40.	2.5	

current speeds and depths considered in this study.

For the 3 ft. and 4 ft. diameter buoys in 5 mph currents, very little change in the results occurred when the scope was reduced from 14.3 to 5.7. Buoy drafts remained nearly the same and, as might be expected, maximum cable tension remained relatively unchanged. Buoy trim angles were reduced from 2 - 12 percent and no excessive cable lengths were noted. This latter condition resulted in very small vertical forces at the anchor (6. - 8. lb.) where there had been 0 vertical force before.

For the 4 ft. diameter buoy at 7 mph reducing the mooring cable scope from 5.6 down to 2.8 resulted in the buoy submerging to its maximum draft. The trim angle remained approximately the same as for the larger scope. However, maximum cable tensions increased from 352 lbs. to 514 lbs.

A similar situation occurs for the 5 ft. diameter buoy. The reduction in scope produces an increase in buoy draft from 1.52 to 1.72 ft.. Maximum cable tension is increased from 350 lbs. to 442 lbs., and there is a significant increase in the vertical force at the anchor (from 49 lbs. to 137 lbs.).

6.3 Effect of Mooring Cable Scope

To verify this influence of the mooring cable scope on cable tension, a small side study outside the basic parametric range was done with the 6 ft. diameter buoy. The 200 lb. configuration with a 12 inch metacentric height and a 60 degree attachment angle was chosen. The two cases

at the highest current speeds were rerun using cable lengths equal to 6 times the stated depth of 25 ft. for the 9 mph case and 40 ft. for the 11 mph case. For the 9 mph case, there was little change in buoy equilibrium trim (a decrease from 22.2 deg. to 21.8 deg.) but maximum cable tensions were reduced from 1820 lbs. to 1730 lbs. The simulated buoy could not achieve moment equilibrium in the 11 mph current.

6.4 Effect of Variation of Cable Diameter

To determine the effect of using a smaller mooring cable diameter on buoy performance, two cases were rerun with a 4 ft. diameter buoy in the 70 lb. configuration with a 4 inch metacentric height and a 60 degree attachment angle. The cases were run in water depths of 7 feet at a current speed of 5 mph and 18 feet at a current speed of 7 mph. A 100-foot long, 1/8 inch diameter cable was used for both. The results are shown in Table 10 below.

TABLE 10
EFFECT OF MOORING CABLE DIAMETER

$d_B = 4.0$ ft., $W_B = 70$ lbs., $GM = 4$ in., $\alpha = 60^\circ$, $l_c = 100$ ft.						
Depth/Current Speed (ft.) (mph)	$d_c = 1/2$ in.			$d_c = 1/8$ in.		
	Max Tension (lbs.)	Draft (ft.)	Trim (deg)	Max Tension (lbs.)	Draft (ft.)	Trim (deg)
7.0/5.0	68.5	0.88	14.6	60.6	0.87	15.5
18.0/7.0	355.3	1.61	17.9	315.9	1.56	18.7

The results indicate that the decrease in cable drag associated with using the smaller diameter cable produces very little change in trim but a slight reduction in draft. The reduction in draft is accompanied by the expected reduction in maximum cable tension. Note that the cable weight in water was unchanged from that used for the 1/2 inch diameter cable. The effect of the cable weight is expected to be very small. Also, no account was taken of the relative stresses produced in these cables by the mooring loads. For this reason, 1/8 inch diameter cable might not be suitable for mooring a 6 ft. diameter buoy in the higher speed current environments.

6.5 Effect of Variation of Cable Drag Coefficient

To determine the influence on buoy-cable performance of a variation in cable drag coefficient, the 4 ft. diameter buoy, used in the cases which examined the influence of cable diameter, was used again. The nominal level of the cable drag coefficient used in the major portion of the parametric studies was a value of $C_R = 1.2$, where C_R is the drag coefficient when the cable is perpendicular to the flow. (The coefficients C_N and C_T are based upon C_R as shown in Section 2.2.) An examination of the open literature on cable drag measurements and the cable characteristics these measurements depend upon revealed that values of C_R could be higher depending upon cable construction. As indicated in Section 6.1, values from 15 to 60 percent larger have been measured.

Based on this information, the value of C_R input to the program was increased from 1.2 to 1.38 and 1.90 and the 4 ft. diameter buoy case mentioned above was rerun at a current speed of 7 mph for these two values of C_R . The results are shown in Table 11 below along with the results obtained at $C_R = 1.2$ for comparison.

TABLE 11
EFFECT OF CABLE DRAG COEFFICIENT

$d_B = 4.0$ ft., $w_B = 70$ lbs., $GM = 4$ inches, $\alpha = 60^\circ$			
$l_c = 100$ ft., water depth = 18 ft., current speed = 7 mph cable diameter = 1/2 in.			
	$C_R = 1.2$	$C_R = 1.38$	$C_R = 1.90$
Max Tension (lb.)	355.3	363.5	386.9
Buoy Draft (ft.)	1.61	1.62	1.65
Buoy Trim (deg.)	17.9	17.8	17.3

It appears that changing the cable drag coefficient does not seriously influence system performance. The biggest effect appears to be in the maximum cable tension, and this is increased by less than 10 percent at the extreme value of C_R .

6.6 Effect of Cable Elasticity

One factor which can effect the performance of the hemispherical buoy-cable system is the elastic property of the cable itself. This influence was not considered in the

parametric studies discussed earlier in Section 6.2. It was incorporated into the mathematical model and the Fast Water Buoy Computer Program after these parametric studies were performed.

To determine the effect on system performance, a few earlier cases were rerun with the influence of cable elasticity included. The cable was assumed to have a circular cross-section corresponding to a 1/2 inch diameter and, in addition, was assumed to have an elastic modulus associated with nylon line. The 6 ft. diameter buoy in the 200 lb. configuration with a 12 inch metacentric height and an attachment angle of 60 degrees was used to make the comparison. The 1/2 inch diameter cable, 100 ft. long was used for the mooring. Its elastic modulus was taken as 13750. lb./in.². Cases were run at current speeds of 5, 7, and 9 mph in corresponding water depths of 7.0, 18.0, and 25.0 ft., respectively. The results and comparison with the earlier results discussed in Section 6.2 are presented in Table 12.

TABLE 12

EFFECT OF CABLE ELASTICITY ON SYSTEM PERFORMANCE

Depth/Current Speed (ft.) (mph)	No Elasticity			With Elasticity		
	Max. Cable Tension (lbs.)	Buoy Draft (ft.)	Buoy Trim (deg.)	Max. Cable Tension (lbs.)	Buoy Draft (ft.)	Buoy Trim (deg.)
7.0/5.0	85.2	0.95	9.8	85.3	0.95	9.9
18.0/7.0	379.7	1.54	14.9	374.5	1.53	15.8
25.0/9.0	1840.8	3.00	22.2	1584.5	2.74	21.9

The results show that when the loads are small to moderate the influence of cable stretch is relatively unimportant in terms of overall system performance. However, in the extreme environment associated with a 9.0 mph current and a short scope, a nylon cable will stretch enough to reduce the cable tension considerably. It is interesting to note that the effect on buoy trim is hardly perceptible.

6.7 Effect of Debris Impingement on System Performance

The last item to be discussed in this section is a very important one from the point-of-view of practical buoy-cable system operations in that it deals with the effect of debris accumulation on buoy-cable performance. Observations in the field have indicated that in the high current environments being considered here, debris will become lodged on the mooring cable, will be driven up the cable by the current, and will accumulate at the buoy-cable attachment point.

Both the mathematical model and the Fast Water Buoy Computer program based upon it consider the presence of such debris. The effect of this type of concentrated load is that it can add a point weight and a point drag to the cable and this, in turn, will produce a discontinuity in both the cable angle with respect to the horizontal ϕ and the cable tension T . The procedure used to determine the magnitude of the change in these quantities at such a point is discussed in detail in Section 2.4.

In order to simulate this effect in the computer program

a separate section in the input routine has been set aside to permit input of the location of the debris along the cable, its weight in water, and its drag constant. In the cases being considered here, the debris is assumed to be at the buoy cable attachment point (i.e., zero location along the cable) and is assumed to be neutrally buoyant. The effect of the drag of the debris is simulated by considering the local cable drag without debris accumulation to be increased by 50 and 100 percent, respectively.

From the results obtained without debris accumulation, the cable angle at the buoy-cable attachment point is known and with this information and the aide of Equations (1), (2), (11), and (12) the normal and tangential cable unit forces can be determined. From them, the cable drag for the no-debris case, D_{CND} , can be calculated. The drag constant for the debris is then estimated from

$$K_a = \frac{D_a}{V_c^2} = \frac{K'D_{CND}}{V_c^2} \quad (37)$$

where K' is the percentage increase in cable drag and is chosen.

A series of cases from the earlier parametric study were rerun with the effect of debris included. The first set was for a 3 ft. diameter buoy in its 50 lb. configuration with a 2 inch metacentric height, a cable attachment angle of 60° , and a cable length and diameter of 100 feet and 1/2 inch, respectively. Only a current speed of 5 mph was considered for this buoy with two values of the parameter K' .

The second set of cases were run for the 6 ft. diameter buoy in the 200 lb. configuration with a metacentric height of 6 inches, and an attachment angle of 60° . Again, a 100 ft. cable length and 1/2 diameter cable were used. Two current speeds were considered, 5 and 7 mph, with two values of the drag percentage parameter K' . The results of this series of cases with the 3 ft. and 6 ft. diameter buoys is presented in Table 13 along with the earlier parametric results, for purposes of comparison.

TABLE 13
EFFECT OF SUBSURFACE DEBRIS ACCUMULATION

$d_B = 3. \text{ ft.}; W_B = 50 \text{ lb.}; GM = 2 \text{ in.}; \alpha = 60^\circ$			
$l_c = 100 \text{ ft.}, d_c = 1/2 \text{ in.}$			
$V_c = 5 \text{ mph}, h = 7. \text{ ft.}$			
	$K' = 0 \text{ (no debris)}$	$K' = 50\%$	$K' = 100\%$
Maximum Cable Tension (lbs.)	72.5	79.8	87.0
Buoy Draft (ft.)	0.95	1.02	1.13
Buoy Trim (deg.)	17.1	16.8	16.5

$d_B = 6. \text{ ft.}; W_B = 200 \text{ lbs.}; GM = 6 \text{ in.}; \alpha = 60^\circ$			
$l_c = 100 \text{ ft.}, d_c = 1/2 \text{ in.}$			
	$K' = 0 \text{ (no debris)}$	$K' = 50\%$	$K' = 100\%$
	$V_c = 5 \text{ mph}; h = 7. \text{ ft.}$		
Maximum Cable Tension (lbs.)	85.3	92.2	98.1
Buoy Draft (ft.)	0.95	0.97	1.01
Buoy Trim (deg.)	12.7	12.4	11.8

$V_c = 7 \text{ mph}; h = 18. \text{ ft.}$			
Maximum Cable Tension (lbs.)	380.	436.	494.
Buoy Draft (ft.)	1.55	1.59	1.66
Buoy Trim (deg.)	15.9	15.8	15.3

AD-A054 507 OCEANICS INC PLAINVIEW N Y F/G 13/10
HYDRODYNAMIC ANALYSIS OF THE PERFORMANCE OF A MOORED HEMISPHERI-ETC(U)
MAY 76 P KAPLAN, J SCHNEIDER, H JASLOW DOT-CG-53393-A
UNCLASSIFIED 76-125 USCZ-D-99-76 NL

20F2
AD
A054507



END
DATE
FILED
7-78
DDC

The results show that the effect of the debris is most pronounced at the higher current speeds. The neutrally buoyant debris always produces a step increase in both the cable angle at the attachment point and the tension at that point. The result is a slight increase in the equilibrium draft of the buoy and a noticeable increase in the maximum cable tension. Interestingly, the buoy equilibrium trim is hardly affected.

One additional case was run to determine the effect on buoy-cable performance of a special type of debris, i.e. a log or branch which becomes lodged on the buoy. This type of debris is not subsurface but rather at the waterline. As such, its influence is not primarily on the cable but rather on the buoy itself.

The log was assumed to be neutrally buoyant and as such its effect was to add to the hydrodynamic drag of the buoy without altering the buoy's hydrodynamic lift or pitching moment. The log was considered to be a solid cylinder with a length of 6 feet and a diameter of 6 inches. Its drag characteristics were estimated with the aid of material in Hoerner [9]. This reference provides data for the drag coefficient of cylinders having various degrees of surface roughness and using this information a drag constant for the log was estimated to be $K_a = 2.4$. (It should be noted that the added drag of the log cannot be applied to the buoy-cable system by means of a simple program input. A special programming modification was required in order to accomplish this.)

The single case run was for the 6 ft. diameter buoy in the 200 lb. configuration with a 6 inch metacentric height and an attachment angle of 60°. The cable length used was 100 ft. and the cable diameter was 1/2 inch. The current speed considered was 7 MPH. The results are shown in Table 14 below along with the corresponding run results from the earlier parameter study.

TABLE 14
EFFECT OF DEBRIS AT THE WATERLINE

$d_B = 6 \text{ ft.}; W_B = 200 \text{ lbs.}; GM = 6 \text{ in.}; \alpha = 60^\circ$		
$l_c = 100 \text{ ft.}, d_c = 1/2 \text{ in.}$		
$V_c = 7 \text{ mph}; h = 18. \text{ ft.}$		
Maximum Cable Tension (lbs.)	Without Surface Debris	With Surface Debris at Waterline
380.	475.	
Buoy Draft (ft.)	1.55	1.61
Buoy Trim (deg.)	15.9	15.6

The results show little if any effect on buoy equilibrium trim and draft. However, a significant increase in cable tension is apparent.

7.0 ADDITIONAL EFFECTS

Among the additional effects that influence the behavior of the hemispherical buoy-cable system are those due to unsteady forces and vortex shedding. A discussion of these quantities is given below.

7.1 Unsteady Forces

The analysis described previously in this report is applied to the steady state configuration of the buoy-cable system, which by definition does not include any unsteady effects. When analyzing such a system, the only expected unsteady effects can be unsteady forces on the buoy itself due to the water flow around it, and any possible unsteadiness in the forces acting on the cable which is often associated with the phenomenon of vortex shedding. With regard to the various hydrodynamic forces on the buoy, any manifestation of unsteady forces of significance would be indicated in the measurements of such forces that were carried out as part of the model tests in the present study. There was no indication in any of the measurements of hydrodynamic lift, drag, or pitching moment of the presence of any periodic effects in the observed measurement traces. The only higher frequency effects recorded were those associated with the general vibratory "noise" due to the towing carriage system, model supports, etc. which were at very high frequency and generally low level relative to the steady forces measured. The test Reynolds Number were sufficiently close to those that would be anticipated in full scale, so that the lack of such unsteady

forces could not be considered a model scale effect. Thus the experimental evidence obtained in this study indicates the lack of any unsteady forces, so that the steady state representation used throughout is appropriate for the present problem of a hemispherical buoy-cable system in a fast current.

7.2 Vortex Shedding

The problem of vortex shedding is generally present whenever fluid moves around a body with a cylindrical section. The occurrence of vortex shedding is associated with a specific value of a non-dimensional frequency parameter, known as the Strouhal Number, which is defined by

$$S = \frac{fc}{V_c} \quad (38)$$

where f = the oscillation frequency associated with the vortex shedding

c = characteristic dimension of the circular section,

V_c = is the characteristic velocity in the present case (current velocity).

The value of $S = 0.2$ is associated with periodic vortex shedding about cylindrical bodies. It is therefore necessary to determine whether there are any basic natural frequencies in the cable system which can be excited by fluid flow, such that when the water flows past the cable section it can excite the system to vibrate in accordance with the Strouhal frequency, as described above.

In order to analyze this problem, a simplified treatment that ignores the hydrodynamic drag forces on the cable will

made, since the natural frequency of the system is basically a function of elastic and mass parameters, with the hydrodynamic drag only expected to act generally as a damping mechanism. The basic unsteady equations are linearized, following the procedure in [14] and using the equations therein. The relations between the perturbed angle of the cable and the velocity of the cable normal to itself (which is the variable of interest wherein oscillations due to vortex shedding are expected to occur) are given by

$$\frac{d\bar{U}}{ds} = - i\omega\bar{\phi} \quad (39)$$

$$\frac{d\bar{\phi}}{ds} = \frac{1}{T_0} \left\{ -i\omega\mu_1\bar{U} - w_c \sin\phi_0 \cdot \bar{\phi} \right\} \quad (40)$$

where ω is the assumed oscillatory frequency (rad./sec.), T_0 is the steady tension, and μ is the sum of the mass and added mass (per unit length) of the cable normal to itself.

These can be combined to give the resultant equation

$$T_0 \frac{d^2\bar{U}}{ds^2} + w_c \sin\phi_0 + \omega^2 \mu_1 \bar{U} = 0 \quad (41)$$

The solution of this equation, which can be used to find the natural frequency (neglecting the term due to the weight), is

$$\bar{U} = A \sin \frac{\omega s}{\sqrt{T_0/\mu_1}}$$

This equation has the boundary conditions

$$\bar{U}(0) = \bar{U}(l) = 0 \quad (42)$$

leading to

$$\frac{\omega l}{\sqrt{T_0/\mu_1}} = \pi \quad (43)$$

which yields the natural frequency for the cable system as

$$f_n = \frac{\sqrt{T_0/\mu_1}}{2l} \quad (44)$$

An evaluation of the Strouhal Number was made for a number of the parameters within the range of the present study, with the largest value found being about 0.02. Thus it appears that there is no vortex shedding occurring due to the flow about the cable in the present situation and that this particular unsteady effect does not play a part in the performance of the hemispherical buoy-cable system when operating in its range of applicability. No evidence of vortex shedding effects appeared in the validation tests, either; which is another indication that unsteady forces do not affect this type of buoy-mooring configuration.

8.0 CONCLUSIONS AND RECOMMENDATIONS

8.1 Conclusions

The two most important design parameters for hemispherical fast water buoys are the buoy trim angle and the maximum cable tension. The objective of keeping the trim angle as small as possible can be achieved by making the attachment angle very large. An attachment angle of 60° was the largest considered in this study and produced, consistently, the lowest trim angles under all conditions investigated. This attachment angle, however, should not be considered an upper limit and higher ones should be investigated.

The use of large attachment angles has, in addition, a side benefit which should be considered. With a large attachment angle, the buoy-cable attachment point can conceivably be out of the water even under deep draft conditions at all but the highest current speeds. This, in effect, could reduce the accumulation of subsurface debris at the attachment point and result in a better chance of survival of the buoy in extreme current environments.

The only other factor which seemed to have a noticeable effect on buoy trim was the metacentric height. Increasing it always tended to reduce the trim, although somewhat less effectively at the higher values of the attachment angle.

Maximum cable tensions, on the other hand, are quite insensitive to cable attachment angle and metacentric height but appear to be affected by buoy weight and by cable length, if sufficient scope is not available. What can be considered

sufficient scope in a fast water environment has not been clearly determined in this limited study but, the results do consistently show that scopes less than 3.0 will produce noticeable increases in maximum cable tensions.

By far the most significant parameter upon which buoy draft and maximum cable tensions depend is the current speed. The increasing current speed induces more hydrodynamic downward lift. This, in turn, increases the buoy draft which increases the hydrostatic buoyant force. However, the increase in relative immersion increases the hydrodynamic lift downward even more. The result is that buoy equilibrium occurs at a deeper level of submergence which results in increased submerged projected area and increased drag. The increased drag, of course, results in a significant increase in the maximum cable tension.

It should be pointed out that not all the buoy configurations tested achieved equilibrium at all current speeds investigated. In fact, none of the configurations could achieve equilibrium in an 11 mph current and only the largest diameter buoy could achieve equilibrium in the 9 mph environment. The smallest diameter studied, the 3 ft. diameter configuration, could not achieve equilibrium at any of the current speeds tested above 5 mph.

To summarize, it appears that any effect which will increase buoy draft (i.e., an increase in buoy weight, too small a mooring cable scope, an increase in hydrodynamic lift due to an increase in current speed) will greatly affect hemispherical buoy-cable system performance. On the other

hand, cable parameters which influence cable drag primarily, do not affect system performance significantly.

8.2 Recommendations

The results obtained from the study of hemispherical buoys in high speed currents presented in this report suggest a number of areas of investigation which should be pursued in any future studies of moored buoys in fast water environments.

These are listed below:

- (1) Hydrodynamic force and moment tests should be expanded to cover the higher Froude number ranges for mid range and high relative immersions. Hydrodynamic force and moment data were taken at 14 fps (i.e., 9.5 mph) only at very low relative immersions. The data seem to indicate that extrapolations to higher Froude numbers may be somewhat risky, particularly for the hydrodynamic pitching moment.
- (2) Computational investigations should be continued into the effects on buoy trim at even higher attachment angles than were considered in this study. The side benefits, as indicated earlier, may be quite important.
- (3) An investigation should be conducted into buoy sizes which will achieve equilibrium trim and draft at Froude numbers corresponding to conditions on either side of the hydrodynamic drag peak. A small change in buoy size may produce a considerable improvement in overall system performance.

9.0 REFERENCES

1. Tozzi, John T.: "A Hemispherical Buoy for Use in the Swift-Running River Environment", Prepared for Dept. of Trans., U.S. Coast Guard; Office of Research and Development, August 1975.
2. Pode, L.: "Tables for Computing and Equilibrium Configuration of a Flexible Cable in a Uniform Stream," David Taylor Model Basin Report No. 687, March 1951.
3. Wilson, B. W.: "Characteristics of Anchor Cables in Uniform Ocean Currents," Texas A&M Research Foundation Report No. 204-1, April 1960.
4. Morrow, B. W. and Chang, W. F.: "Determination of the Optimum Scope of a Moored Buoy," Journal of Ocean Technology, Vol. 2, No. 1, 1967.
5. Schneider, L. and Nickels, F., Jr.: "Cable Equilibrium Trajectory in a Three-Dimensional Flow," ASME Paper No. 66-WA/UNT-12, November 1966.
6. Dale, J. R. and McCandless, J. M.: "Determination of Normal Drag Coefficients for Flexible Cables," U.S. Naval Air Development Center Report No. NADC-AE-6719, June 1967.
7. Reid, R. O.: "Dynamics of Deep-Sea Mooring Lines," Texas A&M University Reference 68-11F, July 1968.
8. Whicker, L. F.: "The Oscillatory Motion of Cable-Towed Bodies," University of California, Institute of Engineering Research, Series 82, Issue 2, May 1957.

9. Hoerner, S. F.: "Fluid-Dynamic Drag," Published by the Author Midland Park, New Jersey, 1958.
10. Sargent, T.P.; Raff, A. I., and Bentson, J.: "Computer Program Documentation Report; Buoy-Cable Dynamics Program," NDBCM 6113.2, Prepared for National Data Buoy Center under Contract NAS8-26879; April 1972.
11. Schneider, J.: "Fast Water Buoy Program Manual," Oceanics Report No. 76-126, March 1976.
12. Pode, L.: "An Experimental Investigation of the Hydrodynamic Forces on Stranded Cables," The David Taylor Model Basin, Report AD 652 335, May 1950.
13. Kelly, R. E. and Goff, C. N.: "Drag and Vibration of Some Wire Ropes and Fairings," United States Navy Mine Defense Laboratory, Research and Development Report I-132, September 1967.
14. Goodman, T.R., Kaplan, P. and Sargent, T.P.: "Static and Dynamic Analysis of a Moored Buoy System," Oceanics Report No. 72-87, January 1972.